Atmos. Meas. Tech. Discuss., 3, 3535–3599, 2010
www.atmos-meas-tech-discuss.net/3/3535/2010/
doi:10.5194/amtd-3-3535-2010

Atmospheric Measurement Techniques Discussions

Determination of aerosol properties from satellite observations of the Ring effect

T. Wagner[1], **S. Beirle**[1], **T. Deutschmann**[2], **and M. P. de Vries**[1]

[1]Max-Planck-Institute for Chemistry, Mainz, Germany
[2]Institute for Environmental Physics, University of Heidelberg, Heidelberg, Germany

Received: 24 July 2010 – Accepted: 5 August 2010 – Published: 19 August 2010

Correspondence to: T. Wagner (thomas.wagner@mpic.de)

Published by Copernicus Publications on behalf of the European Geosciences Union.

Abstract

In this study we explore the potential of satellite observations of the Ring effect (at various wavelengths) for the retrieval of atmospheric aerosol properties. Compared to clouds, aerosols have a rather weak influence on the Ring effect, thus the requirements on the accuracy of the measurements and the radiative transfer simulations are high. In this study, we show that for moderate and high aerosol optical depth (AOD), Ring effect observations are sensitive enough to yield information not only on the AOD, but also on the absorbing properties of aerosols and the aerosol layer height. The latter two quantities are especially important for the determination of the radiative effects of aerosols.

Our investigations are based on observations by the satellite instrument SCIAMACHY on ENVISAT (2004–2008) and on model simulations using the Monte-Carlo radiative transfer model McArtim. In addition to the Ring effect we investigate the impact of aerosols on the absorptions of the oxygen molecule (O_2) and dimer (O_4) as well as the radiance. In general good consistency between measured and simulated quantities is found. In some cases also systematic differences occurred, which are probably mainly related to the strong polarisation sensitivity of the SCIAMACHY instrument.

Our study indicates that Ring effect observations have important advantages for aerosol retrievals: in contrast to O_2 and O_4 absorptions they are only weakly affected by the surface albedo; they can be analysed with high accuracy in various wavelength ranges; and depending on the wavelength range, they show different sensitivities on aerosol properties like single scattering albedo, optical depth or layer height. The results of this study are of particular interest for future satellite instruments with reduced polarisation sensitivity and smaller ground pixels, capable of measuring the Ring effect with higher accuracy.

AMTD

3, 3535–3599, 2010

1 Introduction

The Ring effect describes the so-called "filling-in" of solar Fraunhofer lines in the spectra of scattered sun light compared to direct sun light observations. It was first observed by Shefov (1959) and Grainger and Ring (1962). Today, it is commonly agreed that rotational Raman scattering on atmospheric molecules is the dominant source for the Ring effect (e.g., Kattawar et al., 1981; Solomon et al., 1987). The extent of the filling-in of Fraunhofer lines depends on the number of molecular scatter events, and hence, on the presence and properties of clouds and aerosols. The dominant effect of clouds and aerosols is that they shield the atmosphere below and thus reduce the probability of the observed photons being scattered by air molecules. The occurence of Raman scattering therefore generally decreases with increasing cloud altitude. Several algorithms for the determination of cloud top pressure from satellite observations of the Ring effect were developed in recent years and were successfully applied to observations from the TOMS, GOME, and OMI instruments (Park et al., 1986; Joiner et al., 1995, 2002, 2004; Joiner and Bhartia, 1995; de Beek et al., 2001; Joiner and Vasilkov, 2006; van Deelen et al., 2008; Joiner et al., 2010).

The shielding effect of clouds is also exploited in cloud algorithms based on the absorption of the oxygen molecule O_2 and dimer O_4 (e.g., Kuze and Chance, 1994; Koelemeijer et al., 2001, 2003; de Beek et al., 2001; Acarreta et al., 2004; Kokhanovsky et al., 2005, 2007; Wagner et al., 2008).

In principle, aerosols influence atmospheric radiative transfer in a similar way as clouds do, but the influence of aerosols is usually much weaker, because aerosols usually have much smaller optical depth (AOD) and are typically located close to the surface.

Two basic effects of aerosols can be distinguished (see also Fig. 1)

(a) Albedo effect
Due to the enhanced scattering caused by the aerosol particles, the light path lengths in the lower atmosphere are increased compared to the aerosol-free case.

AMTD
3, 3535–3599, 2010

Since this effect is very similar to the influence of an increased surface albedo it is often referred to as albedo effect. As we will show later, the influence of the albedo effect on the Ring effect is rather weak compared to the absorptions of O_2 and O_4 (see also Sect. 4.3).

(b) Shielding effect
Additional aerosol scattering shields the atmosphere below, leading to a decrease of the strength of the Ring effect and also of trace gas absorptions like those of O_2 and O_4.

In this paper, we systematically investigate the effect of aerosols on various retrieved quantities: besides the Ring effect at different wavelengths, also the absorptions of O_2 and O_4, and on the measured radiance are investigated. Since the observed quantities also strongly depend on the satellite's viewing geometry, the effects of viewing angle and solar zenith angle are also investigated. It should be noted that similar initial studies have been conducted by Vasilkov et al. (2006).

Whenever possible, we use both, measurements and model simulations to determine the dependencies of the observed quantities on aerosol properties and viewing geometry. This is performed for the effects of AOD, aerosol layer height, viewing angle and solar zenith angle. The influence of the aerosol single scattering albedo (SSA) and asymmetry parameter (g) is investigated only by radiative transfer simulations.

The paper is organised as follows: in Sect. 2 information on the SCIAMACHY instrument and the algorithms for the retrieval of the Ring effect, the O_2 and O_4 absorptions, and the normalised radiance is presented. Section 3 introduces the radiative transfer model, which is used for the simulation of the measured quantities. In Sect. 4, the modelled and measured dependencies of the Ring effect and O_2 and O_4 absorptions on the observational geometry (solar zenith angle and viewing angle) and aerosol properties (AOD, SSA, g, and layer height) are discussed. Section 5 presents a summary of the main findings of our study.

AMTD
3, 3535–3599, 2010

2 Instrument and data analysis

We chose observations of the satellite instrument SCIAMACHY on ENVISAT (Burrows et al., 1995; Bovensmann et al., 1999) for this study, because it provides continuous spectra of the earth shine radiance with moderate spectral resolution. Thus the Ring effect can be analysed with high accuracy in different spectral ranges. In addition, absorptions by O_4 and O_2 can be analysed.

It should be noted that continuous spectra with moderate spectral resolution are also available from other satellite instruments like GOME-1 on ERS-2, GOME-2 on METOP, and OMI on AURA. Of these instruments, OMI would be the most suitable for the analysis of the Ring effect, due to its high spatial resolution and the fact that it is almost insensitive to polarisation. However, because the instrument's spectral range ends at 500 nm, no measurement of the O_2 absorption in the red spectral range is possible. We therefore used SCIAMACHY for this study, as it has the next-best spatial resolution.

2.1 SCIAMACHY instrument

In 2002 the SCanning Imaging Absorption SpectroMeter for Atmospheric ChartographY (SCIAMACHY) (Burrows et al., 1995; Bovensmann et al., 1999) was launched on board of ENVISAT. It consists of a set of eight spectrometers that simultaneously measure sunlight reflected from the Earth's surface and atmosphere. SCIAMACHY's eight spectral windows cover the wavelength range between 240 nm and 2380 nm with moderate spectral resolution (0.2–1.2 nm full width at half maximum, FWHM). The satellite operates in a nearly polar, sun-synchronous orbit at an altitude of about 800 km with a local equator crossing time at approximately 10:00 a.m. While the satellite orbits in an almost north-south direction, the SCIAMACHY instrument scans the surface in the perpendicular, east-west direction during daytime. Global coverage is achieved after 6 days at the equator. At higher latitudes better coverage is achieved because of the partial overlap of neighbouring orbits. SCIAMACHY operates in different viewing modes: nadir, limb, and occultation. In the standard operation mode, alternating limb and nadir

AMTD
3, 3535–3599, 2010

measurements are performed. In this study, only nadir observations with a ground pixel size of 30×60 km^2 are used. Due to this rather coarse spatial resolution, the probability for cloud contamination is rather high (Krijger et al., 2007). This constitutes an important limitation for the retrieval of aerosol properties from SCIAMACHY.

Another important property of the SCIAMACHY instrument is its strong polarisation sensitivity. As shown in Fig. 2, this sensitivity varies with wavelength and is especially high in the UV spectral range. Because the spectral features of polarisation and the Ring effect are highly correlated (see e.g., Aben et al., 2003), the retrieval of the Ring effect is affected by the (varying) degree of polarisation of the measured scattered sun light. This problem is further complicated by the fact that the polarisation sensitivity of SCIAMACHY also changes with time.

2.2 Data analysis

The raw satellite spectra are analysed using differential optical absorption spectroscopy (DOAS, see Platt and Stutz, 2008). For the analysis of the Ring effect and of O_2 and O_4 absorption, we selected spectral intervals in which the relevant reference spectrum shows strong and characteristic spectral features. In addition, spectra of all other relevant spectral features in the respective wavelength ranges (trace gas absorptions, Ring spectra, and instrumental features) are included in the spectral fitting procedure. To account for broad band spectral dependencies of surface reflection and scattering on aerosols and cloud particles, a low order polynomial is included. The specific settings and the reference spectra for the different spectral analyses are summarised in Table 1 and described in detail in the following sub-sections.

2.2.1 Ring effect analysis

The analysis of the Ring effect is performed in four different fitting windows in the UV and the blue part of the spectrum, where the filling-in of the solar Fraunhofer lines is particularly strong. The different analyses are referred to as 335 nm, 350 nm, 380 nm,

AMTD
3, 3535–3599, 2010

and 430 nm, according to the centre of the chosen wavelength range, as given in Table 1. Apart from the different wavelength ranges, also different choices of reference spectra are used. For the analyses at 335 nm, 350 nm, and 380 nm more than one Ring spectrum was included in the spectral fitting procedure: in addition to the "standard" Ring spectrum, calculated for a pure Rayleigh scattering atmosphere, a second Ring spectrum representative for the presence of clouds and aerosols was included (for details see Wagner et al., 2009a). For the analyses at 350 nm and 380 nm, a Ring spectrum for vibrational Raman scattering in water was also included (Vasilkov et al., 2002; Vountas et al., 2003). Since these additional Ring spectra show a high degree of correlation to the "standard" Ring spectrum, they were ortho-normalised with respect to the standard Ring spectrum prior to the spectral fitting procedure. This orthonormalisation was performed for the different wavelength ranges in such a way that at the wavelengths of interest (335 nm, 350 nm, 380 nm) the amplitudes of the orthonormalised Ring spectra have their minimum. Thus the fit coefficient of the standard Ring spectrum directly yields the strength of the Ring effect (Wagner et al., 2009a).

For the Ring effect analysis at 430 nm much simpler settings than in the UV were used for two reasons: first, Ring spectral features are mainly present in a small wavelength range below 440 nm. In addition, only few atmospheric absorbers have to be considered in that spectral range. Thus we decided to limit the spectral range to a small fitting window (426–440 nm) and to include only one atmospheric absorber: NO_2. For this small spectral range, the wavelength dependence of the amplitude of the Ring effect is small and thus only one Ring spectrum was included. These simplified settings allowed a very stable and fast algorithm. This algorithm should, however, be used only over the continents, because the Ring spectrum for vibrational Raman scattering in water was not included. Examples of the different Ring analyses are presented in Fig. 3.

The derived fit coefficient of the normalised Ring spectrum directly yields the so-called Raman scattering probability (RSP, see Wagner et al., 2009a), which describes the probability for an observed photon to have been Raman-scattered on air molecules

AMTD
3, 3535–3599, 2010

in the atmosphere. The RSP can directly be compared to the results of the radiative transfer simulations (see Sect. 3). The uncertainty (standard deviation) of the fit results is calculated from the fit residuals. For the Ring analyses it is very small (typically between 1% and 2%).

2.2.2 O_4 analysis

The analysis of the O_4 absorption is performed in the UV and includes two absorption bands (at 360 nm and 380 nm). In principle, O_4 absorption bands in the visible part of the spectrum could also be used (see e.g., Greenblatt et al., 1990). In this study we did not analyse further O_4 bands, because at 477 nm the SCIAMACHY instrument suffers from strong spectral features due to its polarisation sensitivity (see Fig. 2), which interfere with the O_4 analysis. At larger wavelengths (577 nm, 630 nm), spectral interference with strong absorptions of O_2, O_3, and H_2O can lead to problems. These problems might be solved in future analyses by using satellite instruments without pronounced spectral polarisation sensitivities and improved absorption cross sections for the atmospheric O_2 and H_2O absorptions.

The spectral analysis yields the so-called slant column density (SCD), the trace gas concentration integrated along the atmospheric light paths. For the comparison with radiative transfer simulations, the O_4 SCD is divided by the vertically integrated O_4 concentration (vertical column density, VCD), which is calculated from standard temperature and pressure profiles (United States Committee on Extension to the Standard Atmosphere, 1976). In our study, an O_4 VCD of 1.3×10^{43} molec^2/cm^5 was used (for the units of the O_4 column density, see e.g., Greenblatt et al., 1990). The ratio between SCD and VCD yields the air mass factor (AMF):

$$\mathrm{AMF} = \mathrm{SCD}/\mathrm{VCD} \quad (1)$$

It can be directly compared to the AMF derived from the radiative transfer modelling (see Sect. 3). It should be noted that for the O_4 analysis the selected wavelength range includes not only the absorption band at 360 nm but also the weaker absorption band

AMTD
3, 3535–3599, 2010

at 380 nm. This extended wavelength range was chosen to minimise fit uncertainties (which are typically on the order of 5% to 10%). An example for the spectral analysis is presented in Fig. 3.

For the comparison with radiative transfer simulations the choice of a more extended wavelength range leads to a slight inconsistency, because the simulations are performed for only one wavelength, 360 nm. Although the wavelength dependency of the AMF is small (a few percent difference between 360 nm and 380 nm), no exact agreement between measurements and radiative transfer simulations can be expected. Additional discrepancies can be caused by the uncertainty of the O_4 cross section and its temperature dependence (see e.g., Wagner et al., 2009b; Clémer et al., 2010).

2.2.3 O_2 analysis

The O_2 absorption is analysed at 630 nm; details of the analysis can be found in Wagner et al. (2007). An example of the spectral analysis is shown in Fig. 3. The uncertainty of the spectral analysis is typically about 1%. Like for the O_4 analysis, we calculated AMFs from the measured O_2 SCDs using Eq. (1). For the O_2 VCD a value of 4.68×10^{24} molec/cm^2 is used, calculated from pressure and temperature profiles of the US standard atmosphere (United States Committee on Extension to the Standard Atmosphere, 1976). Because of the limited spectral resolution of the SCIAMACHY instrument, the strong and fine-structured atmospheric O_2 absorption can not be fully resolved. Thus a non-linear relationship between the measured absorption (optical depth) and the atmospheric slant column density arises, which is typically referred to as saturation, see e.g., Wagner et al. (2003). In this study we did not correct the saturation effect for the observed O_2 absorptions, but instead applied a respective correction for the results of the radiative transfer simulations (see Sect. 3).

AMTD
3, 3535–3599, 2010

2.2.4 Analysis of the normalised radiance

The SCIAMACHY observations provide spectra of the radiance (R) scattered by the atmosphere and reflected by the Earth's surface and of the direct solar irradiance (I). From these measurements the normalised radiance can be calculated according to the following formula:

$$R_{\text{normalised}} = \frac{R \cdot \pi}{I} \tag{2}$$

For satellite observations the normalised radiance can be interpreted as reflectivity; for a perfectly scattering atmosphere and reflecting earth surface the normalised radiance is unity. We extracted the normalised radiance for most of the wavelengths for which also the Ring effect and the O_2 absorption were analysed: 335 nm, 350 nm, 380 nm, 430 nm, 630 nm. For the extraction of the normalised radiance from SCIAMACHY (including the correction of the polarisation dependence of the instrument), the so-called Müller-matrix approach was used (Lichtenberg et al., 2006).

3 Radiative transfer simulations

The radiative transfer simulations are performed using the full spherical Monte-Carlo radiative transfer model McArtim (Deutschmann, 2009; Deutschmann and Wagner, 2008). The model allows the simulation of ensembles of individual photon trajectories for a given atmospheric situation. From these trajectories the probability of the modelled photons for certain interactions with atmospheric constituents or with the Earth's surface are determined. The scattering events are modelled individually, according to their respective scattering cross sections and phase functions (see Fig. 5). Interaction with the Earth's surface is treated as a Lambertian reflection for a specified ground albedo. In addition to elastic processes (the reflection at the surface, Rayleigh scattering at molecules, and scattering on aerosol and cloud particles), also rotational Raman

AMTD
3, 3535–3599, 2010

scattering events are simulated, allowing to model the Ring effect with McArtim (Wagner et al., 2009a).

Various model runs are performed for different atmospheric scenarios (different aerosol loads and optical properties) and viewing geometries (varying solar zenith angles, viewing angles and relative azimuth angles). The aerosol properties are described by the single scattering albedo (SSA), asymmetry parameter (g, using a Henyey-Greenstein approximation of the aerosol phase function, Henyey and Greenstein, 1941), and vertical profiles of the aerosol extinction. As described in detail in Sect. 4.7, the Ring effect, and the O_2 absorption depend only relatively weakly on the asymmetry parameter (compared to the dependence on other aerosol properties). Thus in most cases, we used a fixed value for g of 0.68. Nevertheless, especially for the radiance and the O_4 absorptions, part of the differences between observations and model simulations might be caused by deviations of the true g from the assumed value of 0.68.

From the model simulations, the normalised radiances, the AMFs for O_4 and O_2 (see Eq. 1), and also the so-called Raman scattering probability (RSP) are obtained (see Sect. 2.2.1). Note that for simplicity, the O_2 AMFs were modelled assuming that O_2 behaves like a weak atmospheric absorber (optical depth$\ll$1), instead of modelling the actual strong and fine-structured atmospheric O_2 absorption. To correct for these assumptions, a subsequent saturation correction was applied to the simulated O_2 AMFs (see Wagner et al., 2003; Grzegorski, 2009), before being compared to the measured O_2 AMF.

4 Sensitivity studies

In this section, we explore the general dependencies of the Ring effect, the O_2 and O_4 absorptions, and the normalised radiances on the observation geometry (solar zenith angle and viewing angle) and aerosol properties (AOD, SSA, g, and layer height).

AMTD
3, 3535–3599, 2010

4.1 Dependence on the solar zenith angle

The interpretation of aerosol effects on satellite observations depends critically on the correct consideration of the observational geometry, especially the dependencies on the solar zenith angle (SZA) and the viewing angle of the instrument. In this sub-section the dependence on SZA is investigated. In Fig. 4 it is shown that the strength of the Ring effect and the O_2 and O_4 absorption increases systematically with increasing SZA at all wavelengths. This dependence is a result of two effects:

(A) Effect of scattering phase function (see Fig. 5)
For singly scattered photons, the scattering angle is determined by the viewing angle and the SZA. For a nadir looking instrument the scattering angle is given by 180°-SZA. Because of the different phase functions for Raman scattering and elastic scattering processes (see Fig. 5, also Kattawar et al., 1981) the probability for Raman scattering (and thus the strength of the Ring effect) increases towards high SZA. For the absorptions of O_4 and O_2, the effect of scattering angle is of minor importance.

(B) Effect of atmospheric path length
The atmospheric light path lengths also increase with increasing SZA, which leads to an increased probability for molecular scattering and absorption. The light path effect is especially important for the O_2 and O_4 absorptions.

It is interesting to note that the relative dependence of the Ring effect and the O_2 and O_4 absorptions on the SZA is similar for all chosen aerosol scenarios. This behaviour allows a rather simple correction of the SZA dependence (see Sect. 4.4).

In Fig. 6 the dependence of the normalised radiance on SZA is shown for various wavelengths and aerosol scenarios. The normalised radiance decreases with increasing SZA for all aerosol scenarios.

We also investigated the SZA dependence based on SCIAMACHY measurements. For that purpose, we selected cloud-free observations at a fixed location. In princi-

AMTD
3, 3535–3599, 2010

ple any location with a pronounced seasonal variation of the SZA would suffice, but for practical reasons we selected SCIAMACHY observations over Beijing, because we also use these observations for the investigation of the dependence on AOD (see Sect. 4.4). In Figs. 7 and 8 the observations of the Ring effect, the O_4 and O_2 absorption, the SZA and the normalised radiance are shown as a function of the time of year. In addition, the modelled SZA dependencies for aerosol-free conditions are shown.

In general, the observed SZA dependence is well described by the model. But also the influence of aerosols can be seen by comparing measured and modelled results: for the observed Ring effect and O_2 absorptions, most values are smaller than the model results (where aerosol-free conditions are assumed). This indicates the importance of the shielding effect on the measured quantities. For the O_4 absorptions also many observations with higher values compared to the model simulations are found. Here, the albedo effect becomes important (see Sect. 1).

For the observed normalised radiances, as expected, in most of the observations the radiances are higher than the model results, which can be explained by the additional scattering by aerosol particles.

In Sect. 4.4 we will use the simulated values (for aerosol-free conditions) to remove the SZA dependence from the observations of the Ring effect and O_4 and O_2 absorptions.

4.2 Dependence on the viewing angle

In addition to the SZA, the viewing angle of the instrument can also have an important effect on the observed quantities. Note that in this study the viewing angle is defined with respect to the horizon: nadir observations are indicated by a viewing angle of -90°; viewing angles $>-90^\circ$ indicate viewing angles towards the east and viewing angles $<-90^\circ$ indicate viewing angles towards the west. In Fig. 9, the simulated dependencies of the Ring effect and the O_4 and O_2 absorptions on the viewing angle are shown. The SZA was set to 30° with the sun shining from the east (like for the SCIAMACHY observations).

AMTD
3, 3535–3599, 2010

For the Ring effect in most cases an increase with increasing viewing angle is found. Like for the dependence on SZA, this can be explained by the direct relationship of the scattering angle to the viewing angle. For increasing viewing angle the scattering angle comes closer to 90° (because the SZA is >0°) and thus the strength of the Ring effect increases (see Fig. 5). It is interesting to note that for small wavelengths, this systematic behaviour is found not only for an aerosol-free case, but also for various aerosol scenarios. In contrast, with increasing wavelength, the dependence of the Ring effect on viewing angle becomes progressively weaker for most aerosol scenarios. For Ring effect observations at 430 nm, even a slight decrease with increasing viewing angle can be found for aerosol scenarios with high AOD, high layer height and high SSA. In these cases, scattering on aerosols becomes the dominant effect (compared to scattering at molecules), and the slight increase of Raman scattering with decreasing viewing angle reflects the decreasing probability for aerosol scattering.

The O_4 absorption at 360 nm increases (slightly) with increasing viewing angle. This increase is mainly related to the decreasing probability for molecular scattering with increasing viewing angle (for the selected SZA). If the probability for molecular scattering decreases, effective light paths become longer, leading to larger O_4 absorptions.

At the wavelength of the O_2 absorption, 630 nm, the probability for Rayleigh scattering is rather small. Most of the observed photons are reflected from the Earth's surface and the atmospheric light path mainly depends on geometry, leading to a mostly symmetrical dependence of O_2 absorption on the viewing angle.

In Fig. 10 the simulated normalised radiances are shown as a function of the viewing angle. For most wavelengths and aerosol cases the normalised radiance increases with decreasing viewing angle, indicating the increased probability of molecular (backward) scattering occurring at scattering angles close to 180°. In some cases, different dependencies are found, especially towards larger wavelengths. In these cases effects with other scattering/reflection probabilities like surface reflection or aerosol scattering dominate the measured radiance.

We also investigated the viewing angle dependencies using observational data. The

AMTD
3, 3535–3599, 2010

search for well-suited satellite observations turned out to be difficult, because for an unambiguous interpretation of the measurements several conditions have to be fulfilled:

- Cloud contamination has to be avoided, since usually the effects of clouds are much larger than those of aerosols.
- Areas with high surface elevation should be avoided, because the Ring effect and O_2 and O_4 absorptions also depend on the terrain height.
- Scenes with high AOD should be avoided to minimise uncertainties of radiative transfer simulations caused by imperfect knowledge of the aerosol properties.
- Observations over oceans should be avoided, because sun glint also has a strong effect on the observed quantities; also water absorption and vibrational Raman scattering might complicate the interpretation of the results.

Based on these conditions we identified a few well suited SCIAMACHY observations, of which one example, in Eastern Europe on 17 September 2006, is shown in Fig. 11. Also displayed are the locations of the SCIAMACHY observations for which the viewing angle dependence is investigated (red box). For these observations the sky was completely cloud-free, and also the aerosol load was rather low: from AERONET observations at Minsk AOD of 0.1 and 0.05 in the UV and red spectral range were observed, respectively. These values for AOD were used in the radiative transfer simulations. Red dots in Fig. 11 indicate fire counts by the MODIS instrument, but these are not relevant to our study.

Figure 12 shows the results of the SCIAMACHY observations of the Ring effect and the O_4 and O_2 absorption, together with results of the radiative transfer simulations. For these simulations, the SZA and viewing geometry corresponding to the SCIAMACHY observations were used.

As expected, the Ring effect observations show a systematic dependence on the viewing angle, which in general is in good agreement with the radiative transfer simulations. However, one exception is found for the Ring effect observations at 350 nm,

AMTD
3, 3535–3599, 2010

which depend only slightly on the viewing angle. This finding is not yet fully understood, but is probably an artefact related to the strong polarisation sensitivity of the SCIAMACHY instrument around 350 nm (see Fig. 2).

Also for the O_2 and O_4 absorptions an overall good agreement between observations and modelling results is found. The differences for the eastern pixels of the SCIAMACHY swath are probably caused by the very low values of the surface albedo at these locations (see Fig. 11). Additional uncertainties might be caused by the fact that the bi-directional reflection function over vegetation is probably not well described by a Lambertian reflector.

Figure 13 shows the observed normalised radiances, together with results of the radiative transfer simulations. While the general dependence on the viewing angle is well reproduced, also a systematic overestimation of the observed radiance by the model simulations towards short wavelengths is obvious. The reason of this overestimation is not completely clear. One reason might again be the influence of the strong polarisation sensitivity of the SCIAMACHY instrument in the UV spectral range (see Fig. 2). In addition, in cases with low surface albedo and low AOD, the deficiencies of a scalar radiative transfer model like McArtim to describe the true atmospheric radiation field might become relatively large (see e.g., Mishchenko et al., 1994). Finally, the assumed low surface albedo (3%) for the simulations might be still too high: like for the O_4 and O_2 absorptions, especially low values in the eastern part of the swath are found, indicating a very low surface albedo. It is interesting to note that from the MODIS observations over this region even small, negative AOD are retrieved on that day (MODIS GIOVANNI product from the NASA Goddard space flight center web site: http://aeronet.gsfc.nasa.gov/cgi-bin/bamgomas_interactive).

4.3 Dependence on the surface albedo

Figure 14 shows the dependence of the Ring effect, the O_2 and O_4 absorptions and the normalised radiance on the surface albedo. The Ring effect for small wavelengths shows almost no dependence on the surface albedo. In contrast, for longer wave-

AMTD
3, 3535–3599, 2010

lengths, the strength of the Ring effect decreases slightly with increasing surface albedo. This behaviour can be understood by the wavelength dependence of molecular scattering: for short wavelengths, each photon that is reflected by the surface, is very probably scattered again by a molecule. Thus the Ring effect depends only weakly on the surface albedo. For larger wavelengths, photons reflected by the surface have a higher probability of reaching the detector without being scattered again by molecules. Thus, with increasing surface albedo the probability of the observed photons to be scattered by molecules slightly decreases.

In contrast, for the O_2 and O_4 absorptions, a strong increase with increasing surface albedo is observed. Here the dominant effect is the increase of the atmospheric light paths with increasing surface albedo, because a larger fraction of the observed photons is scattered at the Earth's surface. The difference of the dependencies of the Ring effect and the O_2 and O_4 absorptions on surface albedo is a very interesting finding and indicates a fundamental advantage of Ring effect observations for the retrieval of aerosol (and cloud) properties. For observations of the O_2 and O_4 absorptions the shielding effect and the albedo effect of aerosols partly cancel each other, leading to an ambiguity in the interpretation of these observations. In contrast, for Ring effect observations, both the shielding effect and the albedo effect typically lead to a decrease of the strength of the Ring effect (with the strongest decreasing albedo effect at small wavelengths).

4.4 Dependence on aerosol optical depth

In this section the dependence of the Ring effect, the O_2 and O_4 absorption and the normalised radiance on the AOD is investigated. For that purpose, SCIAMACHY observations over Beijing were selected. There, often high AOD are found, which allows the study of the effect of aerosols over a large range of AOD. For the characterisation of the AOD we use AERONET data from the station "Beijing" (39.97° N, 116.37° S, http://aeronet.gsfc.nasa.gov/new_web/index.html, see also Holben et al., 2001). This

AMTD
3, 3535–3599, 2010

station provides the best temporal coverage over the selected period from 2004 to 2008. From the AERONET measurements the average AOD during one hour around the time of the SCIAMACHY overpass are calculated. The AOD at 440 nm and 675 nm was directly measured, whereas the AOD at 350 nm was calculated from the other wavelengths based on the Ångström coefficient retrieved for the longer wavelengths. Only measurements of the AOD, for which the standard deviation during the one hour interval was less than 0.3 (at 440 nm) were considered.

The satellite observations were selected according to the following criteria:

- To avoid any influence of bright surfaces due to snow or ice we selected SCIAMACHY observations only for the period from March to September.
- We ensured that the observed scenes were cloud-free from visible inspection of true color images from almost simultaneous observations (time difference 0.5 to 1 h) of the MODIS instrument (MODIS on TERRA, images obtained from NASA/GSFC, MODIS Rapid Response, http://aeronet.gsfc.nasa.gov/cgi-bin/bamgomas_interactive).
- Only SCIAMACHY measurements with the centre of the ground pixel within ±0.15° latitude and ±0.30° longitude around the AERONET station were considered.

In total for the selected period (2004–2008) about 55 pairs of AERONET/SCIAMACHY observations over Beijing fulfilled the selection criteria.

Before comparing the satellite and ground-based data, the effects of varying SZA and viewing geometry have to be considered. The SZA dependence is corrected by simply dividing the observational data by the model results (simulated for aerosol-free scenario) for the respective SZA (see Figs. 7 and 8). For the viewing angle dependence, no such procedure can be performed, because the viewing angle dependence varies systematically with aerosol properties (see Fig. 9). Thus we decided to consider only SCIAMACHY observations for the western and centre part of the swath (viewing

AMTD
3, 3535–3599, 2010

angles $<-81^{\circ}$), for which the viewing angle dependence is relatively small (see Fig. 9). After applying this additional criterion, 37 pairs of AERONET/SCIAMACHY observations were left. Finally, the observations are also corrected for a linear long-term trend, as described in the appendix.

It should be noted that in order to minimise computational effort, the AERONET AOD was not taken at exactly the same wavelength as the SCIAMACHY observations. For the observations of the Ring effect and the O_4 absorption in the UV, the AOD at 350 nm was chosen, whereas for the Ring effect observation at 430 nm and the O_2 absorption at 630 nm, the AOD at 440 nm and 675 nm were taken, respectively. For the comparison to the model simulations, this choice of wavelengths has low impact.

The correlation analyses of the corrected satellite observations of the Ring effect and the O_4 and O_2 absorptions versus the AOD from the AERONET station are shown in the right column of Fig. 15. Please note that the respective correlation analyses for uncorrected data can be found in the Appendix (Figs. B1 and B2). In the left column of Fig. 15, the respective simulation results are presented. To allow a direct comparison between observations and model simulations, the radiative transfer results were also normalised with respect to the values for aerosol-free scenarios (the non-normalised simulation results are shown in Figs. B3 and B4 of the appendix).

For the Ring effect observations (right column in Fig. 15), a negative dependence on the AOD is found for all wavelengths; the strength of this dependence increases towards larger wavelengths. A similar tendency is also found in the model simulations. However, the slope of the modelled dependencies strongly depends on the varied aerosol properties, single scattering albedo and layer height. For short wavelengths, an increase of the Ring effect is even found for purely scattering aerosols at low altitude. In contrast, for large wavelengths a decrease of the Ring effect is found for all assumed aerosol scenarios.

The comparison of observations and simulations indicates that the aerosol over Beijing is typically weakly absorbing (SSA$\approx$0.9). However, again it should be noted that no exact agreement is expected because the simulations were performed for fixed view-

AMTD
3, 3535–3599, 2010

ing geometry (SZA: 30°, viewing angle: −90° (nadir)), while the satellite instrument's observation geometry varies with season.

For the O_4 absorption at 360 nm, a systematic increase with increasing AOD is found. This indicates that for the O_4 absorptions the albedo effect of aerosols usually dominates over the shielding effect. For the O_2 absorptions at 630 nm almost no dependence on the AOD is found, indicating that the albedo effect and shielding effect broadly cancel each other.

In general, the correlations between the satellite data and AOD from the sun photometer observations are rather low (correlation coefficients r^2<0.6). However, this is not too surprising, because the satellite observations do not only depend on the AOD, but also on the layer height and the single-scattering albedo. Also remaining influences of the viewing angle dependence and the horizontal heterogeneity of the aerosol properties might cause part of the variability.

A similar correlation analysis for the observed normalised radiance is shown in Fig. 16. As expected, increasing normalised radiances are found for increasing AOD. The strongest (relative) increase occurs at large wavelengths because there the influence of molecular scattering is much weaker due to the strong wavelength dependence of Rayleigh-scattering. From the comparison between observations and simulations we conclude again that the aerosol over Beijing is typically weakly absorbing with a SSA of about 0.9.

4.5 Dependence on aerosol layer height

Figure 17 presents the dependence of the Ring effect and O_2 and O_4 absorptions on the aerosol layer height derived from radiative transfer simulations. Here, for almost all quantities and aerosol scenarios a negative dependence is found. For the Ring effect this negative dependence is strongest at short wavelengths. At larger wavelengths other aerosol parameters, like SSA and AOD also start playing a role.

A similar dependence exists for the O_4 absorptions at 360 nm, where for all combinations of SSA and AOD decreasing values are found with increasing aerosol layer

AMTD
3, 3535–3599, 2010

height.

The O_2 absorptions show a slightly different behaviour. Only absorbing aerosols cause a decrease with increasing layer height. For purely scattering aerosols, the O_2 absorptions are almost independent on the aerosol layer height.

In Fig. 18 the dependence of the normalised radiance on the aerosol layer height is shown. As expected for purely scattering aerosols the radiance almost does not depend on the layer height. In contrast, for absorbing aerosols, a systematic decrease of the radiance with increasing layer height is found. This decrease is caused by the absorption of photons which have been scattered by molecules inside the aerosol layer. With increasing vertical extent of the aerosol layer, a higher number of such photons are absorbed, and are thus not observed by the satellite instrument. This effect is more pronounced in the UV where the scattering by molecules is much more probable compared to larger wavelengths.

In addition to the sensitivity studies based on radiative transfer simulations, we also searched for observational data to investigate the dependence on the aerosol layer height. One criterion for this search was the availability of (almost) coincident observations from the CALIOP instrument, from which information on the aerosol layer height can be derived (e.g., Winker et al., 2009).

We especially looked for individual CALIOP observations showing strong variations oft the layer height over small distances, in order to minimise possible complications due to variations of the observational geometry and aerosol properties. Another criterion was the presence of high AOD to ensure a strong effect on the satellite observations. Thus the search was focussed on the Beijing area, because of the high AOD expected there. We identified one interesting example (area south of Beijing, 16 September 2006), for which the above mentioned conditions were fulfilled. MODIS observations are used to ensure that the selected area is nearly free of clouds (see Fig. 19). From sun photometer measurements at the AERONET station in Beijing and from MODIS observations the AOD was found to range between 2 and 3. From CALIOP measurements at around 05:30 UTC we estimate an

AMTD
3, 3535–3599, 2010

increase in aerosol layer height from about 1 km at 40° N to about 2.5 km altitude at 37° N (http://www-calipso.larc.nasa.gov/products/lidar/browse_images/production/). The track of the CALIOP overpass is indicated by the black line in Fig. 19. From the SCIAMACHY observations we chose only the eastern part of the swath (with the same viewing angles for all latitudes) to minimise the influence of the viewing angle on the analysed quantities. The selected SCIAMACHY ground pixels are indicated by the red box in Fig. 19.

The results of the Ring effect and the O_2 and O_4 absorptions for the selected SCIAMACHY observations are shown in Fig. 20. Also shown are results from radiative transfer simulations assuming a linear increase of the aerosol layer height from 1 to 2.5 km between 40° N and 37° N. The SSA was set to 0.95, and the AOD was set to 3 for wavelengths in the UV and blue spectral range and to 1.5 for 630 nm. Note that these aerosol properties can of course be only a rough representation for the true values, especially because of the rather large time difference between the SCIAMACHY and CALIOP observations (about 3.5 h).

For the Ring effect, a general decrease with increasing layer height is found at all wavelengths. However, at short wavelengths, the model simulations systematically overestimate the observations. Part of this discrepancy might be related to the strong polarisation sensitivity of the SCIAMACHY instrument. Another reason for this discrepancy might be an increasing AOD and/or decreasing SSA with decreasing wavelength (see also Sect. 4.6). For the Ring effect observations at 380 nm and 430 nm a local minimum around 1.5 km altitude is observed, which is probably related to an increase of the AOD at these locations (the sensitivity of the Ring effect to AOD increases with wavelength, see Fig. 15). Indications for locally increased AOD are also found from other observations (see below).

Besides these deviations, the systematic dependence on layer height is in general well described by the simulations using the assumed aerosol properties.

For the O_2 and O_4 absorptions no clear dependencies on the aerosol layer height are observed. This indicates the competing influences of the shielding effect and albedo

AMTD
3, 3535–3599, 2010

effect. For aerosol altitudes around 1.5 km, both the O_2 and O_4 absorptions show local maxima, also indicating an increased AOD at these locations, maybe due to the presence of thin clouds.

In Fig. 21, the dependence of the observed and simulated normalised radiances on layer height is presented. Overall good agreement is found, especially taking into account the fact that the true AOD (and SSA and g) is not known. Around a layer height of 1.5 km enhanced values of the normalised radiance are found confirming the assumption of a locally increased AOD. In contrast, the rather low values at about 1 km indicate that the AOT at these locations might be smaller than assumed in the radiative transfer simulations.

4.6 Dependence on aerosol single scattering albedo

The sensitivity of the observations to the aerosol single scattering albedo (SSA) is investigated using radiative transfer simulations. The respective results of the Ring effect and the O_4 and O_2 absorption are shown in Fig. 22. For the Ring effect, a (positive) dependence on the SSA is found only at small wavelengths (335 and 350 nm). The reason is that a layer of absorbing aerosols shields the atmosphere below it from view of the satellite instrument, thereby decreasing the Raman scattering probability for the observed photons. In contrast, non-absorbing aerosols tend to increase the Raman scattering probability, because after being scattered by an aerosol particle, the photon is very likely to be scattered again by a molecule due to the high probability of molecular scattering at short wavelengths.

In contrast, Ring effect observations at larger wavelengths depend only weakly on the aerosol SSA. For these wavelengths, the effect of absorbing aerosols is similar compared to shorter wavelengths. But now, due to the decreased probability of molecular scattering, non-absorbing aerosols also tend to decrease the Raman scattering probability. Thus the influence of the aerosol SSA on the Ring effect is much weaker at larger wavelengths (380 and 430 nm) compared to short wavelengths.

For the absorptions of O_2 and O_4, an increase with increasing SSA is found for all

AMTD
3, 3535–3599, 2010

aerosol scenarios. With decreasing aerosol SSA the probability for photons from low atmospheric layers to reach the satellite instrument decreases, shortening the average light path length, and leading to decreased absorption by O_4 and O_2.

For the observed radiance, shown in Fig. 23, a strong increase with increasing aerosol SSA is found. The strongest (relative) dependence occurs for large wavelengths, for which the scattering on molecules is relatively weak.

4.7 Dependence on aerosol asymmetry parameter

The sensitivity of the observations to the aerosol asymmetry parameter (g) is also investigated using radiative transfer simulations. The effect of the aerosol asymmetry parameter to the observed quantities is similar to that of the aerosol single scattering albedo. With increasing g (or decreasing SSA) less radiation is directly backscattered to the satellite sensor. Thus especially the observed radiance depends strongly on the aerosol g (and aerosol SSA), see Fig. 25. Nevertheless, there is also an important difference between the effects of aerosol g and SSA: while for SSA<1 photons are absorbed an thus removed from the radiation field, the variation of g only affects the distribution of atmospheric light paths. Thus in general for the Ring effect and the absorptions of O_2 and O_4 weaker dependencies are found compared to the influence of the aerosol SSA (see Fig. 24).

5 Conclusions

In this study we explored the potential of satellite observations of the Ring effect to retrieve aerosol properties. Compared to clouds, the influence of aerosols on the Ring effect is rather weak because the optical depth of aerosols is usually much smaller than that of clouds. In addition, atmospheric aerosols are usually located at low altitude and therefore shield only a small fraction of the total atmospheric column. Fortunately, the Ring effect is a rather strong signal in the UV spectral range and thus can be typically

AMTD
3, 3535–3599, 2010

analysed with high accuracy.

In addition to the observations of the Ring effect at various wavelengths (335 nm, 350 nm, 380 nm, and 430 nm), we also investigated observations of the atmospheric absorptions of O_4 (at 360 nm) and O_2 (at 630 nm) and the normalised radiance (at 335 nm, 350 nm, 380 nm, 430 nm, and 630 nm). Like the Ring effect, these observations are systematically affected by the presence of aerosols (see e.g., Kokhanovsky et al., 2010).

We analysed observations of the satellite instrument SCIAMACHY on ENVISAT, because it provides continuous spectra of the earth shine radiance with moderate spectral resolution over a large wavelength range.

However, the SCIAMACHY instrument also has some significant limitations: first, the spectral features of polarisation and the Ring effect are highly correlated (see e.g., Aben et al., 2003), and therefore the retrieval of the Ring effect is affected by the (varying) degree of polarisation of the measured scattered sun light. This problem is further complicated by the fact that the polarisation sensitivity of SCIAMACHY changes with time. Second, due to the rather large ground pixel size ($30 \times 60\,km^2$) the probability for cloud contamination is high. Despite these limitations, a clear influence of aerosols on SCIAMACHY observations was found in this study. In general, the observations agree well with model simulations.

From our observations we derive the following main conclusions:

- Observations of the Ring effect depend on several aerosol properties like AOD, single scattering albedo, phase function, and layer height.
- Depending on the selected wavelength range, Ring effect observations are especially sensitive to specific aerosol properties: at short wavelengths, they depend mainly on layer height and SSA; at large wavelengths they depend mainly on AOD.
- In contrast to observations of the O_2 and O_4 absorption, the influence of surface albedo on the Ring effect is only weak.

AMTD
3, 3535–3599, 2010

– Usually the strength of the Ring effect can be analysed with high accuracy (on the order of 1% or below). Unfortunately, due to the strong polarisation sensitivity of the SCIAMACHY instrument this advantage could not be fully exploited in this study.

– For observations of the O_2 and O_4 absorption the shielding effect and albedo effect of aerosols have opposing effects, often (partly) compensating each other. Thus the interpretation of such observations is rather ambiguous. In contrast, for Ring effect observations the shielding effect and albedo effect work in the same direction, thus aerosols typically lead to a decrease of the Ring effect in satellite observations.

Our study indicates that Ring effect observations might be very well suited for the retrieval of aerosol properties from space. From the synergistic use of Ring effect analyses at different wavelengths it should be possible to extract different aerosol properties like AOD, single scattering albedo and layer height. Similar conclusions were also derived by Vasilkov et al. (2006). If possible, also further quantities like the normalised radiance or the absorptions of O_4 and O_2 should be simultaneously analysed and used in the aerosol retrieval.

As already pointed out, SCIAMACHY observations are not ideal for the analysis of the Ring effect. But improved accuracy is expected from future satellite instruments if they are less sensitive to polarisation and have reduced ground pixel size. This would make satellite observations of the Ring effect, possibly in combination with observations of the O_2 and O_4 absorptions and the normalised radiance, a powerful tool for global observations of aerosol properties.

AMTD
3, 3535–3599, 2010

Appendix A

Quantification and correction of the long term trend

This appendix contains some details about the (linear) correction of the long term trends affecting the satellite observations. Figures A1 and A2 present time series of the Ring effect, the O_2 and O_4 absorption and the normalised radiance over Beijing for the period 2004–2008. The data show a seasonal cycle mainly caused by the variation of the SZA over the measurement location, but in addition it shows a long term trend, which is especially strong for the Ring effect observations in the UV. The long term trend is quantified by fitting a linear regression line to the time series and is subsequently corrected by subtracting the fitted trend from the measurements. One explanation for the observed trend of the Ring effect is the strong polarisation sensitivity of the SCIAMACHY instrument, since the spectral polarisation of the observed radiance shows a high correlation with the spectral shape of the Ring spectrum (Aben et al., 2003). This hypothesis is confirmed by the fact that the largest long term trends are found for Ring effect observations in the UV, where the polarisation sensitivity of the SCIAMACHY instrument is particularly strong (see also Fig. 2).

Although SCIAMACHY radiances and irradiances are also known to degrade significantly during the time range studied here, the time trend found for the reflectances is small because data were used that were corrected with the M-factors (Noël, 2005).

Appendix B

Raw data for the investigation of the aerosol optical depth dependence

The investigation of the dependencies of the observed quantities on aerosol optical depth (AOD) is complicated by the interference with the influence of additional dependencies. First, for the selected measurements (especially for the Ring effect obser-

AMTD
3, 3535–3599, 2010

vations in the UV) a long term trend is found, which is corrected as described in the Appendix A. Second, the SZA changes systematically with season (see Fig. 8). The SZA dependence is corrected by dividing the measured data by results from radiative transfer simulations (for the aerosol-free case) for the corresponding SZA (see Figs. 7 and 8). Third, also the viewing angle has a strong effect on the observed quantities. In contrast to the SZA dependence, this effect can not be easily corrected, because the viewing angle dependence is different for different aerosol properties. We minimised the viewing angle dependence by excluding observations at the most eastern pixels (with viewing angle smaller than -81°). In Figs. B1 and B2 we show correlation analyses of the measured data versus the AERONET AOD for the different processing steps of the measured data. The raw measurement data are shown in the left columns, the data after correction of the long-term trend and the SZA dependence are shown in the middle columns, and the data after most eastern satellite pixels are excluded are shown in the right columns.

To allow a rather direct comparison of the measurements with simulated data, also the results of the radiative transfer simulations are normalised. For that purpose all simulation results are divided by the values for AOD of zero. The normalised results are shown in Figs. 15 and 16. in the main part of the paper; the corresponding original simulation results are shown in Figs. B3 and B4.

Acknowledgements. We used several external data sets in this study and we want to thank especially the following persons and institutions: Hong-Bin Chen, Philippe Goloub, and Anatoli Chaikovsky for their efforts in establishing and maintaining the Beijing and Minsk AERONET sites. MODIS images were obtained from NASA/GSFC, MODIS Rapid Response, http://aeronet.gsfc.nasa.gov/cgi-bin/bamgomas_interactive. CALIOP data were taken from http://www-calipso.larc.nasa.gov/products/lidar/browse_images/production. We want to thank Ralf Snel and Ilse Aben for fruitful discussions.

The service charges for this open access publication have been covered by the Max Planck Society.

AMTD
3, 3535–3599, 2010

References

Aben, I., Tanzi, C. P., Hartmann, W., Stam, D. M., and Stammes, P.: Validation of space-based polarization measurements by use of a single-scattering approximation, with application to the global ozone monitoring experiment, Appl. Optics, 42, 3610–3619, 2003.

Acarreta, J. R., de Haan, J. F., and Stammes, P.: Cloud pressure retrieval using the O_2-O_2 absorption band at 477 nm, J. Geophys. Res., 109, doi:10.1029/2003JD003915, 2004.

Bogumil, K., Orphal, J., Homann, T., Voigt, S., Spietz, P., Fleischmann, O. C., Vogel, A., Hartmann, M., Bovensmann, H., Frerik, J., and Burrows, J. P.: Measurements of molecular absorption spectra with the SCIAMACHY pre-flight model: instrument characterization and reference data for atmospheric remote-sensing in the 230–2380 nm region, J. Photochem. Photobiol. A, 157, 167–184, 2003.

Bovensmann, H., Burrows, J. P., Buchwitz, M., Frerick, J., Noël, S., Rozanov, V. V., Chance, K. V., and Goede, A. H. P.: SCIAMACHY – mission objectives and measurement modes, J. Atmos. Sci., 56(2), 127–150, 1999.

Burrows, J. P., Hölzle, E., Goede, A. P. H., Visser, H., and Fricke, W.: SCIAMACHY – scanning imaging absorption spectrometer for atmospheric chartography, Acta Astronaut., 35(7), 445, 1995.

Clémer, K., Van Roozendael, M., Fayt, C., Hendrick, F., Hermans, C., Pinardi, G., Spurr, R., Wang, P., and De Maziére, M.: Multiple wavelength retrieval of tropospheric aerosol optical properties from MAXDOAS measurements in Beijing, Atmos. Meas. Tech., 3, 863–878, doi:10.5194/amt-3-863-2010, 2010.

de Beek, R., Vountas, M., Rozanov, V. V., Richter, A., and Burrows, J. P.: The Ring effect in the cloudy atmosphere, Geophys. Res. Lett., 28, 721–724, 2001.

van Deelen, R., Hasekamp, O. P., van Diedenhoven, B., and Landgraf, J.: Retrieval of cloud properties from near ultraviolet, visible and near infrared satellite-based Earth reflectance spectra: a comparative study, J. Geophys. Res., 113, D12204, doi:10.1029/2007JD009129, 2008.

Deutschmann, T.: Atmospheric radiative transfer modelling using Monte Carlo methods, Diploma thesis, University of Heidelberg, 2008.

Deutschmann, T. and Wagner, T.: TRACY-II Users manual, http://joseba.mpch-mainz.mpg.de/Strahlungstransport.htm, 2008.

Grainger, J. F. and Ring, J.: Anomalous Fraunhofer line profiles, Nature, 193, 762, 1962.

AMTD
3, 3535–3599, 2010

Greenblatt, G. D., Orlando, J. J., Burkholder, J. B., and Ravishankara, A. R.: Absorption measurements of oxygen between 330 and 1140 nm, J. Geophys. Res., 95, 18577–18582, 1990.
Grzegorski, M.: Cloud retrieval from UV/VIS satellite instruments (SCIAMACHY and GOME), PhD-thesis, University of Heidelberg, Germany, 2009.
Henyey, L. and Greenstein, J.: Diffuse radiation in the galaxy, Astrophys. J., 93, 70–83, 1941.
Holben, B. N., Tanre, D., Smirnov, A., Eck, T. F., Slutsker, I., Abuhassan, N., Newcomb, W. W., Schafer, J., Chatenet, B., Lavenue, F., Kaufman, Y. J., Vande Castle, J., Setzer, A., Markham, B., Clark, D., Frouin, R., Halthore, R., Karnieli, A., O'Neill, N. T., Pietras, C., Pinker, R. T., Voss, K., and Zibordi, G.: An emerging ground-based aerosol climatology: Aerosol Optical Depth from AERONET, J. Geophys. Res., 106, 12067–12097, 2001.
Hsu, N. C., Herman, J. R., Bhartia, P. K., Seftor, C. J., Torres, O., Thompson, A. M., Gleason, J. F., Eck, T. F., and Holben, B. N.: Detection of biomass burning smoke from TOMS measurements, Geophys. Res. Lett., 23(7), 745–748, 1996.
Joiner, J. and Bhartia, P. K.: The determination of cloud pressures from rotational Raman scattering in satellite backscatter ultraviolet measurements, J. Geophys. Res., 100, 23019–23026, 1995.
Joiner, J., Vasilkov, A., Flittner, D., Buscela, E., and Gleason, J.: Retrieval of Cloud Pressure from Rotational Raman Scattering, in: OMI Algorithm Theoretical Basis Document Vol. III: Clouds, Aerosols, and Surface UV Irradiance, edited by: Stammes, P., ATBD-OMI-03, Version 2.0, Aug 2002, http://www.knmi.nl/omi/documents/data/OMI_ATBD_Volume_3_V2.pdf, 31–46, 2002.
Joiner, J., Vasilkov, A. P., Flittner, D. E., Gleason, J. F., and Bhartia, P. K.: Retrieval of cloud pressure and oceanic chlorophyll content using Raman scattering in GOME UV measurements, J. Geophys. Res., 109, D01109, doi:10.1029/2003JD003698, 2004.
Joiner, J. and Vasilkov, A. P.: First results from the OMI rotational Raman scattering cloud pressure algorithm, Geosci. Remote Sens., IEEE Transactions, 44(5), 1272–1282, 2006.
Joiner, J., Vasilkov, A. P., Bhartia, P. K., Wind, G., Platnick, S., and Menzel, W. P.: Detection of multi-layer and vertically-extended clouds using A-train sensors, Atmos. Meas. Tech., 3, 233–247, doi:10.5194/amt-3-233-2010, 2010.
Joiner, J., Bhartia, P. K., Cebula, R. P., Hilsenrath, E., McPeters, R. D., and Park, H.: Rotational Raman scattering – Ring effect in satellite backscatter ultraviolet measurements, Appl. Optics, 34, 4513–4525, 1995.
Kattawar, G. W., Young, A. T., and Humphreys, T. J.: Inelastic-scattering in planetary-

AMTD
3, 3535–3599, 2010

atmospheres, 1. The Ring effect, without aerosols, Astrophys. J., 243(3), 1049–1057, 1981.
Koelemeijer, R. B. A., Stammes, P., Hovenier, J. W., and de Haan, J. F.: A fast method for retrieval of cloud parameters using oxygen a band measurements from the Global Ozone Monitoring Experiment, J. Geophys. Res., 106, 3475–3490, 2001.
Koelemeijer, R. B. A., de Haan, J. F., and Stammes, P.: A database of spectral surface reflectivity in the range 335–772 nm derived from 5.5 years of GOME observations, J. Geophys. Res., 108(D2), 4070, doi:10.1029/2002JD002429, 2003.
Kokhanovsky, A. A., Rozanov, V. V., Burrows, J. P., Eichmann, K.-U., Lotz, W., and Vountas, M.: The SCIAMACHY cloud products: algorithms and examples from ENVISAT, Adv. Space Res., 36, 789–799, 2005.
Kokhanovsky, A. A., Mayer, B., Rozanov, V. V., Wapler, K., Burrows, J. P., and Schumann, U.: The influence of broken cloudiness on cloud top height retrievals using the nadir observations of backscattered solar radiation in the oxygen A-band, J. Quant. Spectrosc. Ra., 103, 460–477, 2007.
Kokhanovsky, A. A. and Rozanov, V. V.: The determination of the dust cloud altitude from a satellite using hyperspectral measurements in the gaseous absorption band, Int. J. Remote Sens., 31 , 10, 2729-2744, 2010.
Krijger, J. M., van Weele, M., Aben, I., and Frey, R.: Technical Note: The effect of sensor resolution on the number of cloud-free observations from space, Atmos. Chem. Phys., 7, 2881–2891, doi:10.5194/acp-7-2881-2007, 2007.
Kuze, A. and Chance, K. V.: Analysis of cloud top height and cloud coverage from satellites using the O_2 A and B bands, J. Geophys. Res., 99, 14481–14491, 1994.
Levelt, P. F., Hilsenrath, E., Leppelmeier, G. W., van den Oord, G. H. J., Bhartia, P. K., Tamminen, J., de Haan, J. F., and Veefkind, J. P.: Science objectives of the ozone monitoring instrument, IEEE Trans. Geosci. Remote Sens., 44(5), 1199–1208, doi:10.1109/TGRS.2006.872336, 2006.
Lichtenberg, G., Kleipool, Q., Krijger, J. M., van Soest, G., van Hees, R., Tilstra, L. G., Acarreta, J. R., Aben, I., Ahlers, B., Bovensmann, H., Chance, K., Gloudemans, A. M. S., Hoogeveen, R. W. M., Jongma, R. T. N., Nol, S., Piters, A., Schrijver, H., Schrijvers, C., Sioris, C. E., Skupin, J., Slijkhuis, S., Stammes, P., and Wuttke, M.: SCIAMACHY Level 1 data: calibration concept and in-flight calibration, Atmos. Chem. Phys., 6, 5347–5367, doi:10.5194/acp-6-5347-2006, 2006.
Meller, R. and Moortgat, G. K.: Temperature dependence of the absorption cross sections of

AMTD
3, 3535–3599, 2010

formaldehyde between 223 and 323 K in the wavelength range 225–375 nm, J. Geophys. Res., 105, 7089–7101, 2000.
Mishchenko, M. I., Lacis, A. A., and Travis, L. D.: Errors induced by the neglect of polarization in radiance calculations for Rayleigh-scattering atmospheres, J. Quant. Spectrosc. Ra., 51, 491–510, doi:10.1016/0022-4073(94)90149-X, 1994.
Noël, S.: Determination of Correction Factors for SCIAMACHY Radiances and Irradiances, technical documentation, Institute for Environmental Physics, University of Bremen, Document number: IFE-SCIA-SN-20050203_IrrRadCorrection, http://www.iup.physik.uni-bremen.de/sciamachy/SCIA_CAL/irrad_corr.pdf, 2005.
Park, H., Heath, D. F., and Mateer, C. L.: Possible application of the Fraunhofer line filling in effect to cloud height measurements, Meteorological Optics, OSA Technical Digest Series, 70–81, Opt. Soc. Am., Washington, DC, 1986.
Penning de Vries, M. J. M., Beirle, S., and Wagner, T.: UV Aerosol Indices from SCIAMACHY: introducing the SCattering Index (SCI), Atmos. Chem. Phys., 9, 9555–9567, doi:10.5194/acp-9-9555-2009, 2009.
Rothman, L. S., Jacquemart, D., Barbe, A., Benner, D. C., Birk, M., Brown, L. R., Carleer, M. R., Chackerian Jr, C., Chance, K., Coudert, L. H., Dana, V., Devi, V. M., Flaud, J.-M., Gamache, R. R., Goldman, A., Hartmann, J.-M., Jucks, K. W., Maki, A. G., Mandin, J.-Y., Massie, S. T., Orphal, J., Perrin, A., Rinsland, C. P., Smith, M. A. H., Tennyson, J., Tolchenov, R. N., Toth, R. A., Vander Auwera, J., Varanasi, P., and Wagner, G.: The HITRAN 2004 molecular spectroscopic database, J. Quant. Spectrosc. Ra., 96, 139–204, 2005.
Shefov, N. N.: Spectroscopic, photoelectric, and radar investigations of the aurora and the nightglow, Izd. Akad. Nauk., 1, 25–28, 1959.
Slijkhuis, S.: SCIAMACHY level 0 to 1c processing algorithm theoretical basis document, Tech. Note ENV-ATB-DLR-SCIA-0041, Dtsch. Zent. für Luft- und Raumfahrt, Oberpfaffenhofen, Germany, 1999.
Solomon, S., Schmeltekopf, A. L., and Sanders, R. W.: On the interpretation of zenith sky absorption measurements, J. Geophys. Res., 92, 8311–8319, 1987.
United States Committee on Extension to the Standard Atmosphere, US Standard Atmosphere, 1976, National Oceanic and Atmospheric Administration, National Aeronautics and Space Administration, United States Air Force, Washington DC, 1976.
Vandaele, A. C., Hermans, C., Simon, P. C., Carleer, M., Colin, R., Fally, S., Merienne, M. F., Jenouvrier, A., and Coquart, B.: Measurements of the NO_2 absorption cross-section from

AMTD
3, 3535–3599, 2010

42 000 cm^{-1} to 10 000 cm^{-1} (238–1000 nm) at 220 K and 294 K, J. Quant. Spectrosc. Ra., 59, 171–184, 1998.
Vasilkov, A. P., Joiner, J., Gleason, J., and Bhartia, P. K.: Ocean Raman scattering in satellite backscatter UV measurements, Geophys. Res. Lett., 10, 29, 1833, doi:10.1029/2002GL014955, 2002.
Vasilkov, A. P., Joiner, J., Bhartia, P. K., Torres, O., and Spurr, R.: Using Rotational Raman Scattering in the Atmosphere for Satellite Retrieval of the Aerosol Plume, AGU Spring Meeting Abstracts, http://adsabs.harvard.edu/abs/2006AGUSM.A34A..02V, 2006.
Vountas, M., Richter, A., Wittrock, F., and Burrows, J. P.: Inelastic scattering in ocean water and its impact on trace gas retrievals from satellite data, Atmos. Chem. Phys., 3, 1365–1375, doi:10.5194/acp-3-1365-2003, 2003.
Wagner, T., Heland, J., Zöger, M., and Platt, U.: A fast H_2O total column density product from GOME – Validation with in-situ aircraft measurements, Atmos. Chem. Phys., 3, 651–663, doi:10.5194/acp-3-651-2003, 2003.
Wagner, T., Beirle, S., Deutschmann, T., Grzegorski, M., and Platt, U.: Satellite monitoring of different vegetation types by differential optical absorption spectroscopy (DOAS) in the red spectral range, Atmos. Chem. Phys., 7, 69–79, doi:10.5194/acp-7-69-2007, 2007.
Wagner, T., Beirle, S., Deutschmann, T., Grzegorski, M., and Platt, U.: Dependence of cloud properties derived from spectrally resolved visible satellite observations on surface temperature, Atmos. Chem. Phys., 8, 2299–2312, doi:10.5194/acp-8-2299-2008, 2008.
Wagner, T., Beirle, S., and Deutschmann, T.: Three-dimensional simulation of the Ring effect in observations of scattered sun light using Monte Carlo radiative transfer models, Atmos. Meas. Tech., 2, 113–124, doi:10.5194/amt-2-113-2009, 2009.
Wagner, T., Deutschmann, T., and Platt, U.: Determination of aerosol properties from MAX-DOAS observations of the Ring effect, Atmos. Meas. Tech., 2, 495–512, doi:10.5194/amt-2-495-2009, 2009.
Winker, D. M., Vaughan, M. A., Omar, A., Hu, Y., Powell, K. A., Liu, Z., Hunt, W. H., and Young, S. A.: Overview of the CALIPSO mission and CALIOP data processing algorithms, J. Atmos. Ocean. Tech., 26, 2310–2323, 2009.
Wilmouth, D. M., Hanisco, T. F., Donahue, N. M., and Anderson, J. G.: Fourier transform ultraviolet spectroscopy of the $A^2\Pi_{3/2} \leftarrow X^2\Pi_{3/2}$ transition of BrO, J. Phys. Chem., 103, 8935–8944, 1999.

AMTD
3, 3535–3599, 2010

Table 1. Overview on the selected parameters for the different spectral analyses.

Analysis	Wavelength range (nm)	Degree of polynomial	Reference spectra	Preparation	Source
Ring effect 335 nm	325–344	4	standard Ring[1]		direct sun spectrum
			cloud Ring[1]		direct sun spectrum
			NO_2 220 K	convolution	(Vandaele et al., 1998)
			O_3 221 K	convolution	(Bogumil et al., 2003)
			O_3 241 K	convolution	(Bogumil et al., 2003)
			KAPPA_NAD	interpolation	instrument keydata[2]
			OBM_s_p	interpolation	instrument keydata[2]
Ring effect 350 nm	340–360	3	standard Ring		direct sun spectrum
			cloud Ring		direct sun spectrum
			vibrational Ring		T. Kurosu[6]
			NO_2 220 K	convolution	(Vandaele et al., 1998)
			HCHO 298 K	convolution	(Meller et al., 2000)
			BrO 228 K	convolution	(Wilmouth et al., 1999)
			O_3 221 K	convolution	(Bogumil et al., 2003)
			O_3 241 K	convolution	(Bogumil et al., 2003)
			O_4 296 K	interpolation	(Greenblatt et al., 1990)
			KAPPA_NAD	interpolation	instrument keydata[2]
			OBM_s_p	interpolation	instrument keydata[2]
Ring effect 380 nm	370–390	3	standard Ring		direct sun spectrum
			cloud Ring		direct sun spectrum
			vibrational Ring		T. Kurosu[6]
			NO_2 220 K	convolution	(Vandaele et al., 1998)
			O_3 221 K	convolution	(Bogumil et al., 2003)
			O_4 296 K	interpolation	(Greenblatt et al., 1990)
			KAPPA_NAD	interpolation	instrument keydata[2]
			OBM_s_p	interpolation	instrument keydata[2]
Ring effect 430 nm	426–440		standard Ring		direct sun spectrum
			NO_2 220 K	convolution	(Vandaele et al., 1998)
O_4 360 nm[3]	353–390	3	same as Ring effect 380 nm	same as Ring effect 380 nm	same as Ring effect 380 nm
O_2 630 nm	614–683.2	3	standard Ring		direct sun spectrum
			O_2 290 K	convolution	HITRAN data base[4]
			O_4 290 K	interpolation	(Greenblatt et al., 1990)
			H_2O	convolution	HITRAN data base[4]
			inverse I_o–spectrum		direct sun spectrum
			grass	interpolation	ASTER library[5]
			conifers	interpolation	ASTER library[5]
			decidous	interpolation	ASTER library[5]
			ZETA_NAD	interpolation	instrument keydata[2]
			OBM_s_p	interpolation	instrument keydata[2]

[1] see Sect. 2.2.1; [2] http://www.iup.physik.uni-bremen.de/sciamachy/SCIA_CAL/rad_cal.html; [3] For simplicity the two band analysis (360 nm and 380 nm) is referred to as 360 nm analysis throughout the study, the O_4 cross section was scaled by 1.3, see (Wagner et al., 2009b); (Clémer et al., 2010); [4] (Rothman et al., 2004); [5] http://speclib.jpl.nasa.gov/; [6] personal communication, 2008

AMTD
3, 3535–3599, 2010

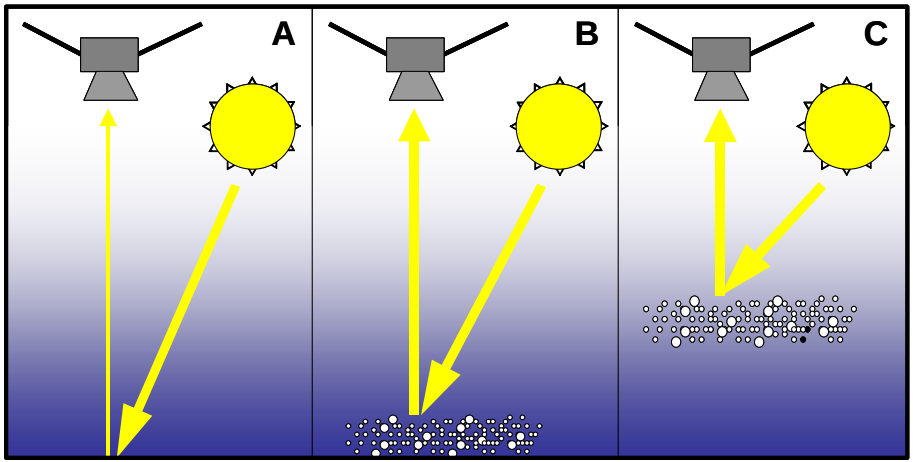

Fig. 1. Basic effects of aerosols on the atmospheric radiative transfer. Albedo effect: compared to an aerosol-free atmosphere (left figure), in the presence of aerosols the effective earth's albedo is increased leading to a higher probability of the observed photons to have "seen" the lower atmosphere (centre figure). Shielding effect: additional scattering by aerosols causes a reduction of the light path lengths below the aerosol layer (right figure).

AMTD
3, 3535–3599, 2010

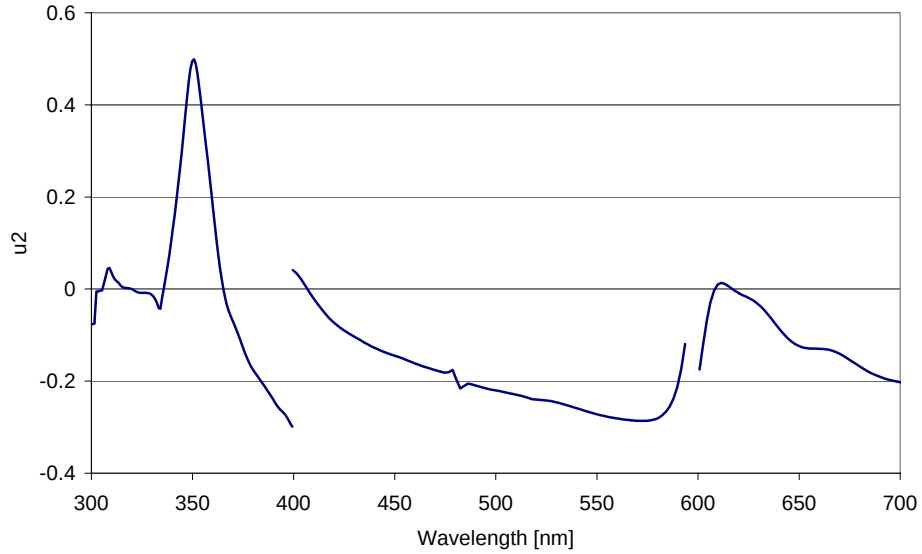

Fig. 2. Illustration of the wavelength dependent polarisation sensitivity of the SCIAMACHY instrument. Displayed is the so-called u2-vector, the ratio of the Müller matrix elements for one polarisation direction and unpolarised light (Slijkhuis et al., 1999). The u2 vector is based on the version 3.1 keydata (Noël et al., 2005).

AMTD
3, 3535–3599, 2010

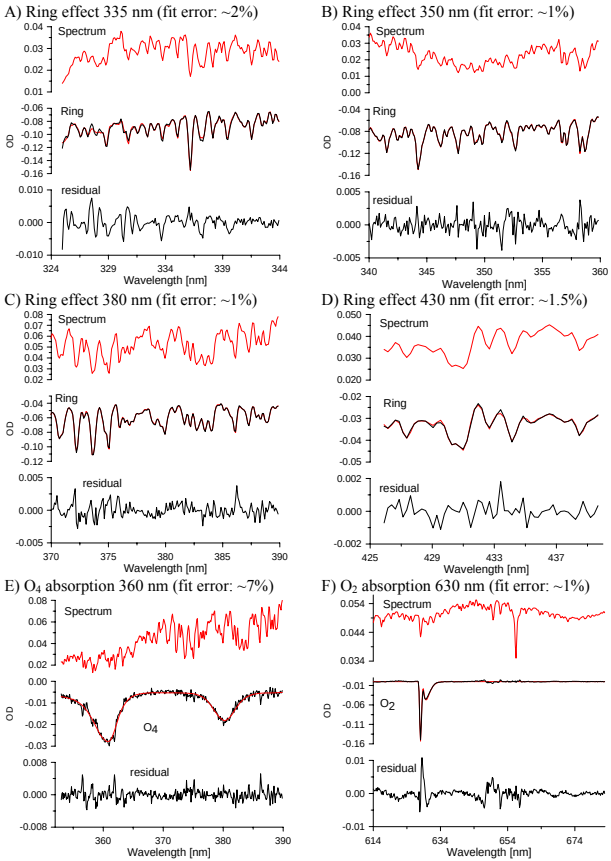

Fig. 3. Fit results of the spectral analyses of the Ring effect in different wavelength ranges **(A–D)** and the O_2 and O_4 absorptions **(E, F)**. In each graph, the top panels show the measured raw spectra; the middle panels show the respective reference spectra (red) and the retrieved signature from the spectral analysis (black); the bottom panels show the spectral residuals.

AMTD
3, 3535–3599, 2010

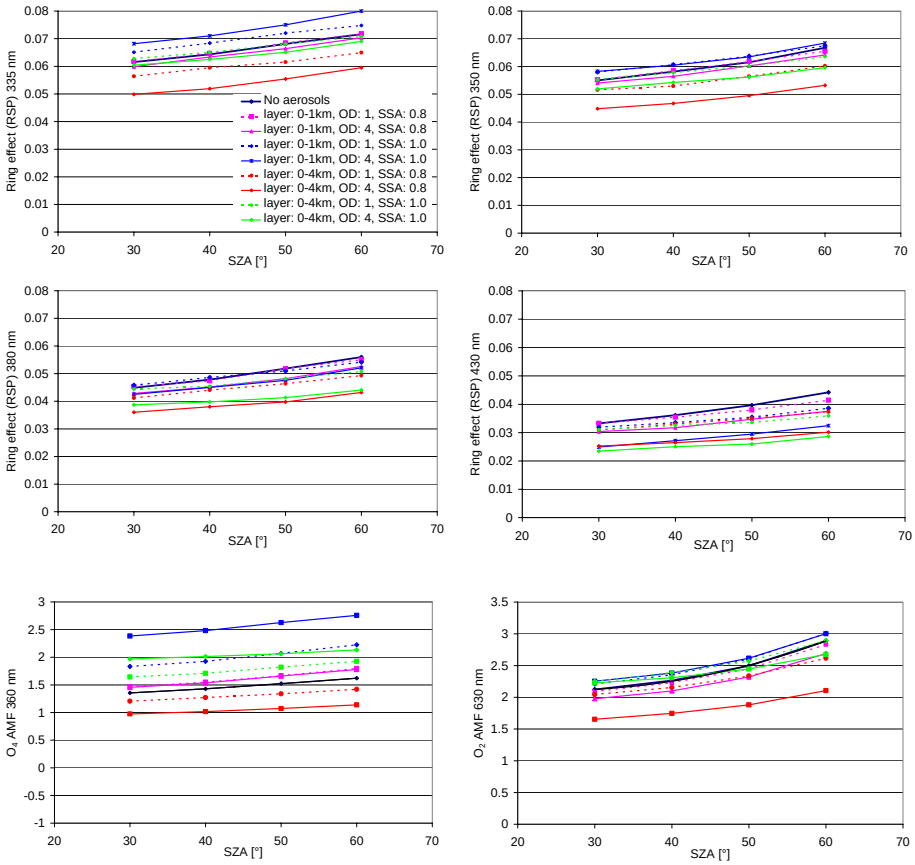

Fig. 4. Modelled dependence of the Ring effect and the O_2 and O_4 absorptions on the solar zenith angle. The calculations are performed for a viewing angle of −90° (nadir geometry), aerosol asymmetry parameter of 0.68, and surface albedo of 10% for 630 nm and 5% for all other wavelengths.

AMTD
3, 3535–3599, 2010

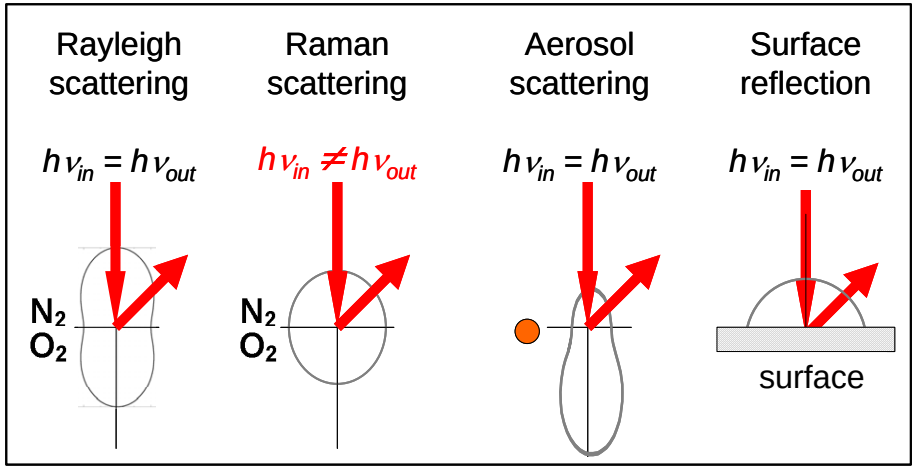

Fig. 5. Angular dependence of different types of scattering and reflection. Compared to Rayleigh scattering and aerosol scattering the angular dependence of rotational Raman scattering is weak. Thus, for a scattering angle of 90° the relative contribution of Raman scattering (and thus the Ring effect) is strongest.

AMTD
3, 3535–3599, 2010

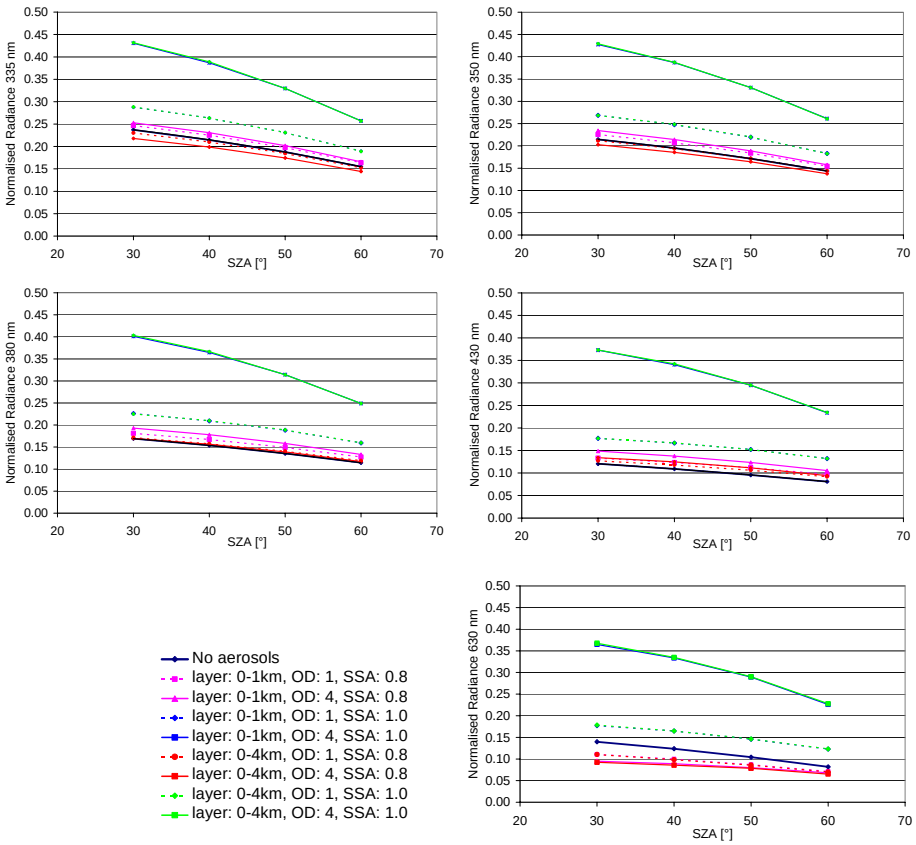

Fig. 6. Dependence of the normalised radiance on the solar zenith angle. The calculations are performed for a viewing angle of −90° (nadir geometry), aerosol asymmetry parameter of 0.68, and surface albedo of 10% for 630 nm and 5% for all other wavelengths.

AMTD
3, 3535–3599, 2010

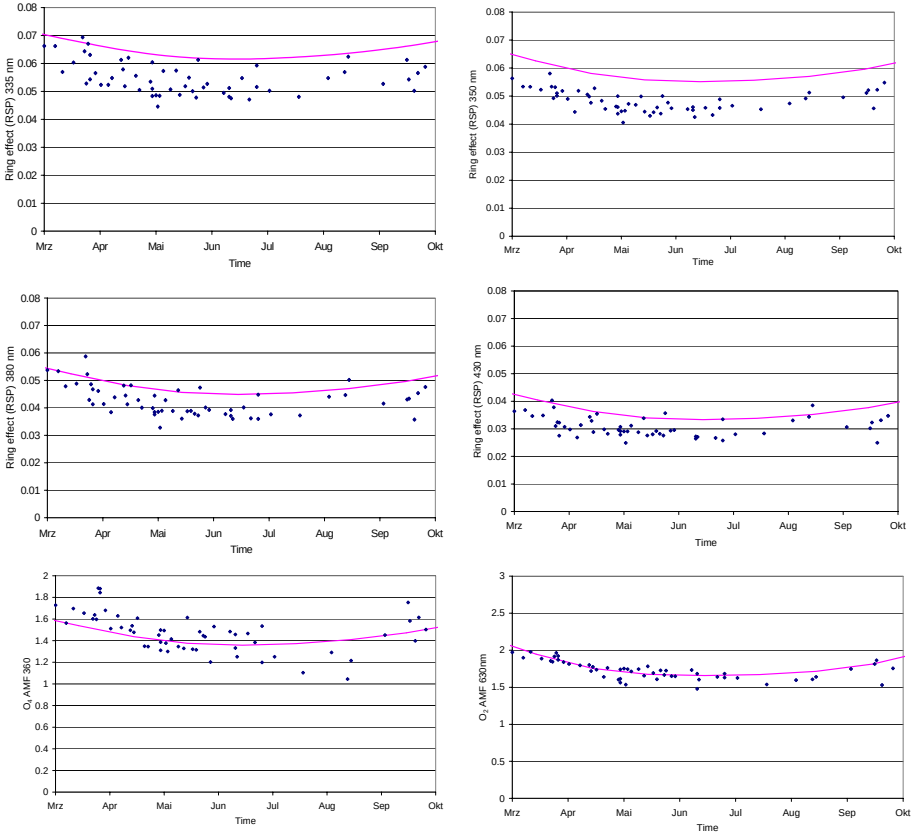

Fig. 7. Seasonal variation (March–October) of the Ring effect and O_2 and O_4 absorption over Beijing. The measurements include only cloud-free observations. The magenta lines represent the result of radiative transfer simulations (see Sect. 3) for aerosol-free conditions. For 630 nm the surface albedo was set to 10%; for all other wavelengths it was set to 5%.

AMTD
3, 3535–3599, 2010

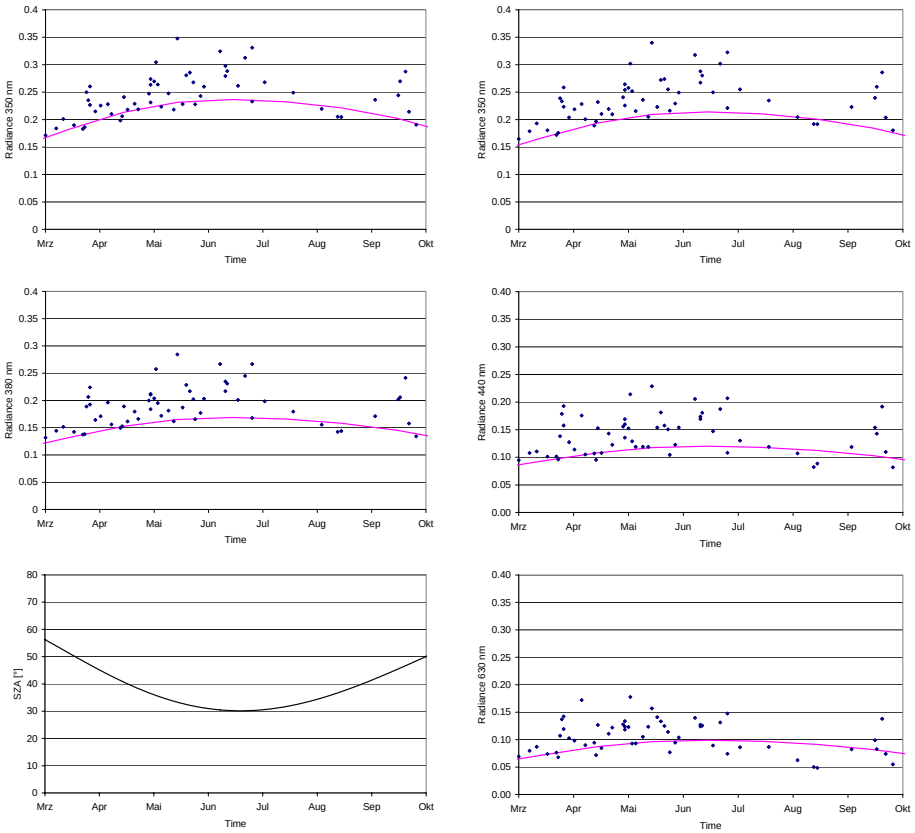

Fig. 8. Seasonal variation (March–October) of the normalised radiances over Beijing. The measurements include only cloud-free observations. The magenta lines represent the result of radiative transfer simulations (see Sect. 3) for aerosol-free conditions. Also shown is the seasonal variation of the SZA (lower left panel). For 630 nm the surface albedo was set to 10%; for all other wavelengths it was set to 5%.

AMTD
3, 3535–3599, 2010

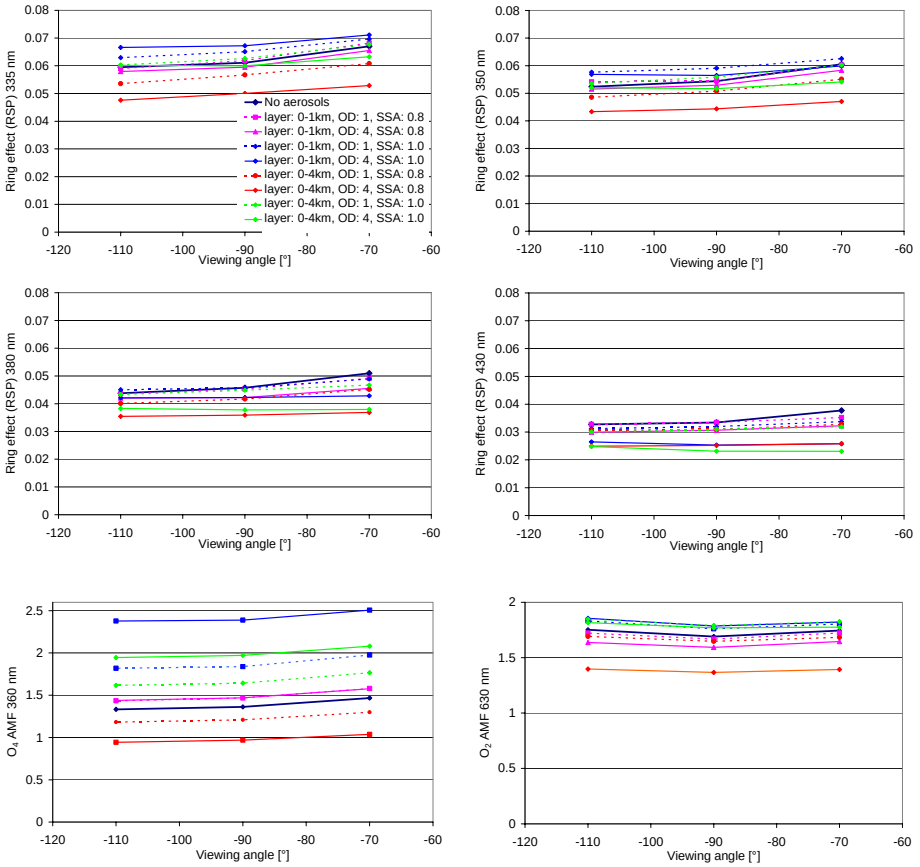

Fig. 9. Dependence of the Ring effect and the O_2 and O_4 absorptions on the viewing zenith angle of the satellite instrument (angles larger than −90° indicate eastern direction). The calculations are performed for SZA of 30° with the sun in eastern direction. For 630 nm the surface albedo was set to 10%; for all other wavelengths it was set to 5%. The aerosol asymmetry parameter was assumed to be 0.68.

AMTD
3, 3535–3599, 2010

Aerosol retrievals from Satellite Ring effect observations

T. Wagner et al.

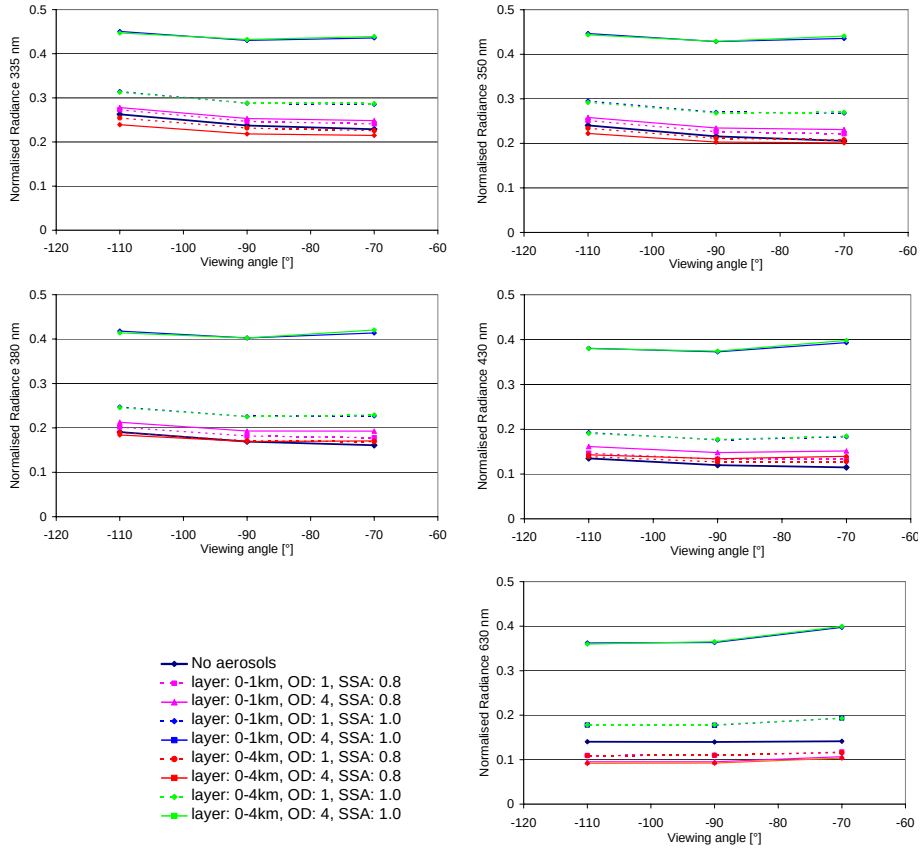

Fig. 10. Dependence of the normalised radiances on the viewing zenith angle of the satellite instrument (angles larger than −90° indicate eastern direction). The calculations are performed for SZA of 30° with the sun in eastern direction. For 630 nm the surface albedo was set to 10%; for all other wavelengths it was set to 5%. The aerosol asymmetry parameter was assumed to be 0.68.

AMTD
3, 3535–3599, 2010

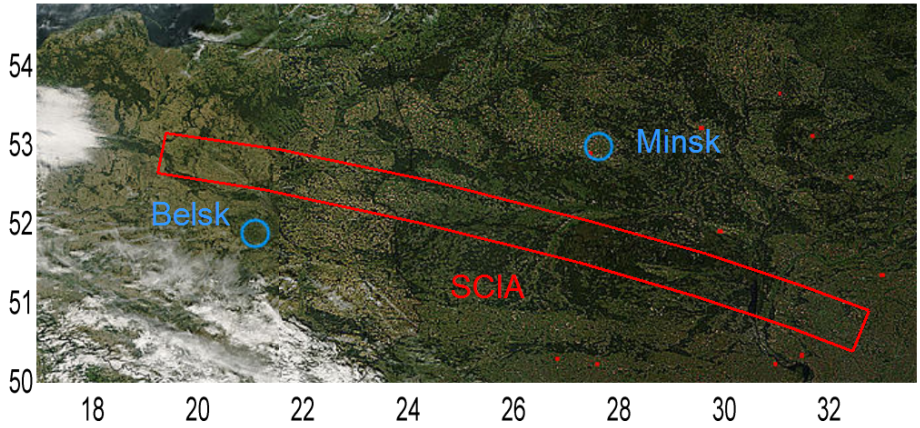

Fig. 11. MODIS RGB image over Eastern Europe on 17 September 2006. On this day, the sky was almost cloud-free and very low AOD (below 0.1 in the UV) were measured by an AERONET station in Minsk (marked with a blue circle). The red lines indicate the location of two west-east scanning sequences of the SCIAMACHY instrument on that day. Red dots in the figure indicate MODIS fire counts, but they are ignored here. The observed Ring effect, O_4 and O_2 absorption, as well as the normalised radiances for these measurements are shown in Figs. 12 and 13.

AMTD
3, 3535–3599, 2010

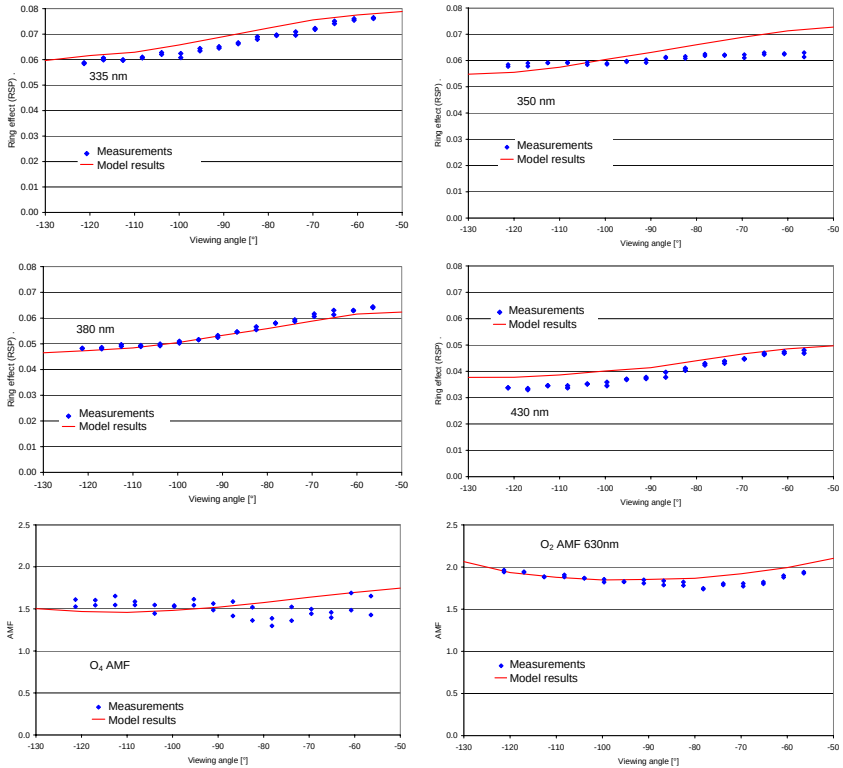

Fig. 12. Observed (blue dots) and modelled dependency of the Ring effect and the O_4 and O_2 absorption on the viewing angle for selected cloud-free observations (results of two consecutive SCIA scans) over Eastern Europe (17 September 2006, see Fig. 11). The deviations of the measured O_4 and O_2 absorptions from the simulated values are probably related to variations of the surface albedo. For the radiative transfer calculations the following parameters were assumed: surface albedo: 3%, the aerosol layer: 0–1 km; aerosol SSA: 0.95; g: 0.68, AOD: 0.05 (630 nm) and 0.1 (all other wavelengths). A viewing angle of −90° indicates nadir viewing geometry.

AMTD
3, 3535–3599, 2010

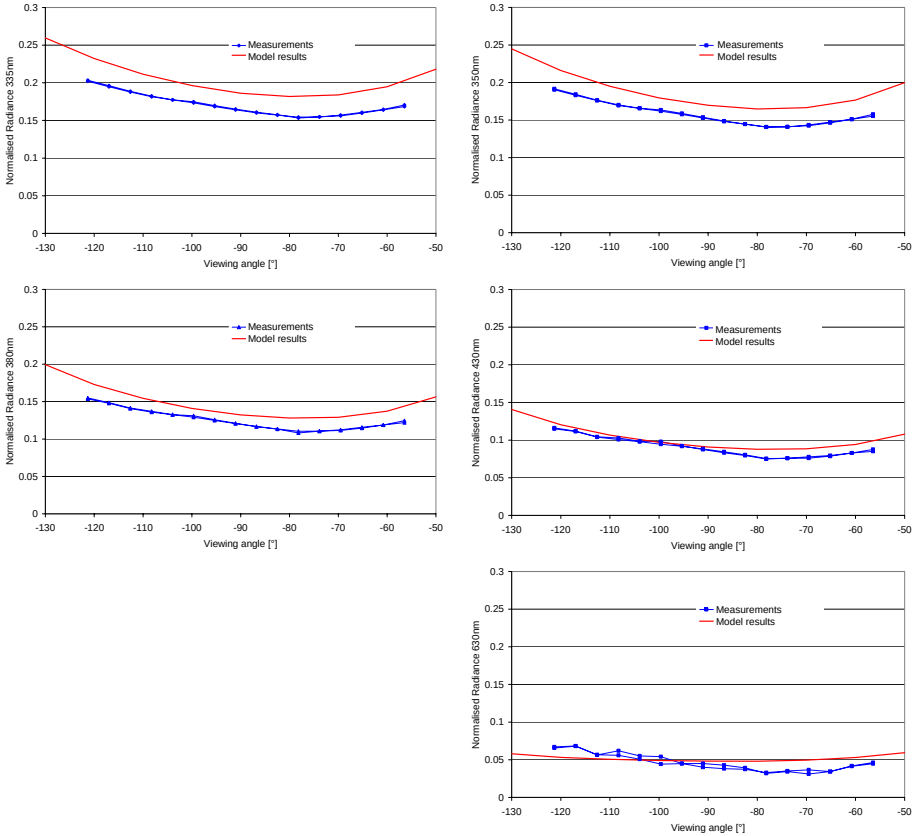

Fig. 13. Observed (blue dots) and modelled dependency of the normalised radiance on the viewing angle for selected cloud-free observations (results of two consecutive SCIA scans) over Eastern Europe (17 September 2006, see Fig. 11). For the radiative transfer calculations the following parameters were assumed: surface albedo: 3%, the aerosol layer: 0–1 km; aerosol SSA: 0.95; g: 0.68, AOD: 0.05 (630 nm) and 0.1 (all other wavelengths). A viewing angle of −90° indicates nadir viewing geometry.

AMTD
3, 3535–3599, 2010

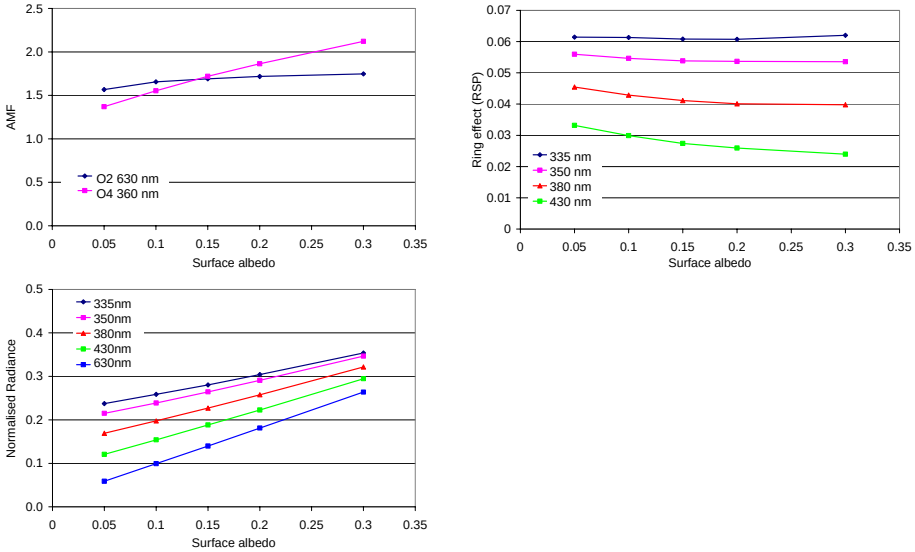

Fig. 14. Dependence of the Ring effect, the O_2 and O_4 absorption and the normalised radiance on the surface albedo. The calculations are performed for SZA of 30° and a viewing angle of −90° (nadir geometry).

AMTD
3, 3535–3599, 2010

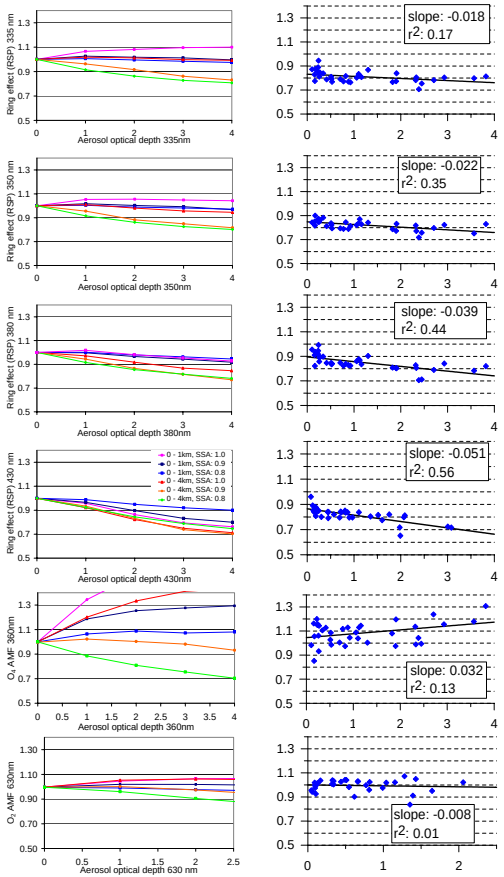

Fig. 15. Observed (right) and simulated (left) dependence of the Ring effect and the O_2 and O_4 absorptions on the AOD. The data are normalised to model results for an AOD of 0 (see text). The calculations are performed for SZA of 30° and a viewing angle of −90° (nadir). The aerosol asymmetry parameter was assumed to be 0.68.

AMTD
3, 3535–3599, 2010

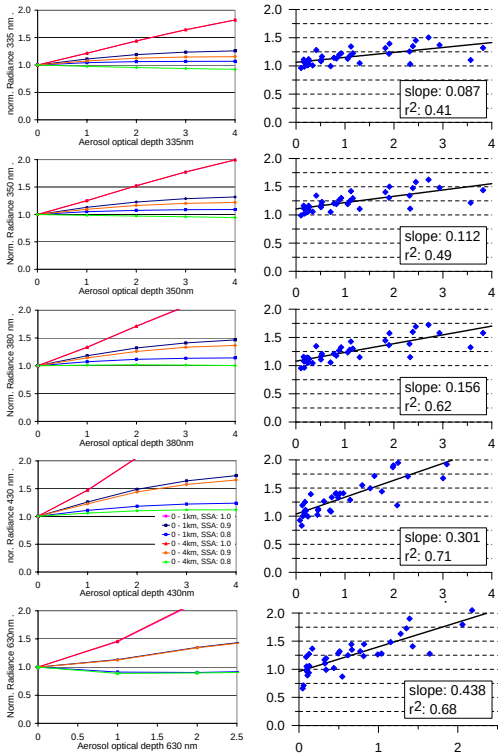

Fig. 16. Observed (right) and simulated (left) dependence of the normalised radiance on the AOD. The data are normalised to the values modelled for an AOD of 0 (see text). The calculations are performed for SZA of 30° and a viewing angle of −90° (nadir). The aerosol asymmetry parameter was assumed to be 0.68.

AMTD
3, 3535–3599, 2010

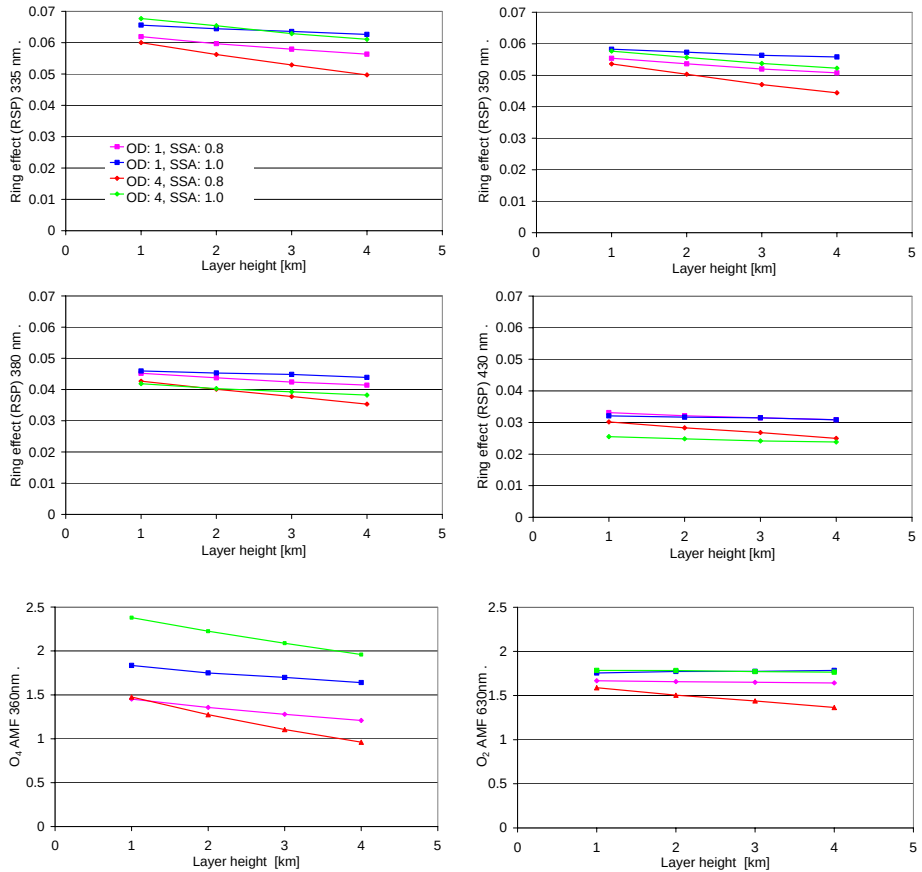

Fig. 17. Dependence of the Ring effect and the O_2 and O_4 absorptions on the aerosol layer height (the *x*-axis indicates the upper boundary of the aerosol layer; the lower boundary is the surface). The calculations are performed for SZA of 30° and a viewing angle of −90° (nadir). The aerosol asymmetry parameter was assumed to be 0.68.

AMTD
3, 3535–3599, 2010

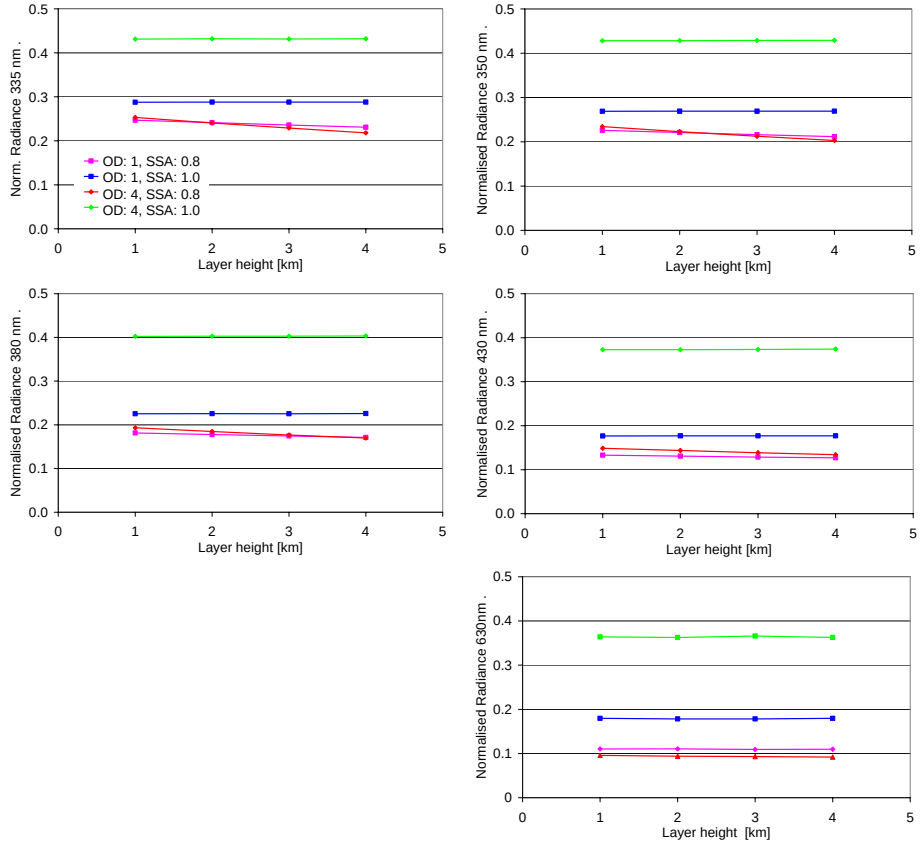

Fig. 18. Dependence of the normalised radiance on the aerosol layer height (the x-axis indicates the upper boundary of the aerosol layer; the lower boundary is the surface). The calculations are performed for SZA of 30° and viewing angle of −90° (nadir). The aerosol asymmetry parameter was assumed to be 0.68.

AMTD
3, 3535–3599, 2010

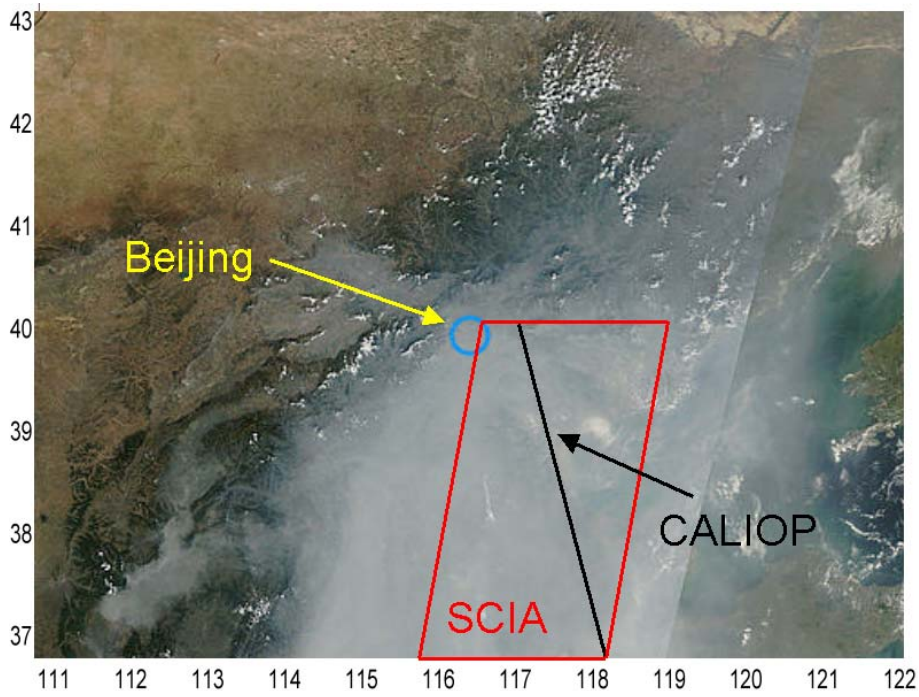

Fig. 19. MODIS RGB image for a day with strong aerosol pollution (16 September 2006) over the area around over Beijing (AOD between 2 and 3). Near-simultaneous CALIOP measurements indicate that the aerosol layer height between about 40° N and 37° N increased from about 1 km to 2.5 km.

AMTD
3, 3535–3599, 2010

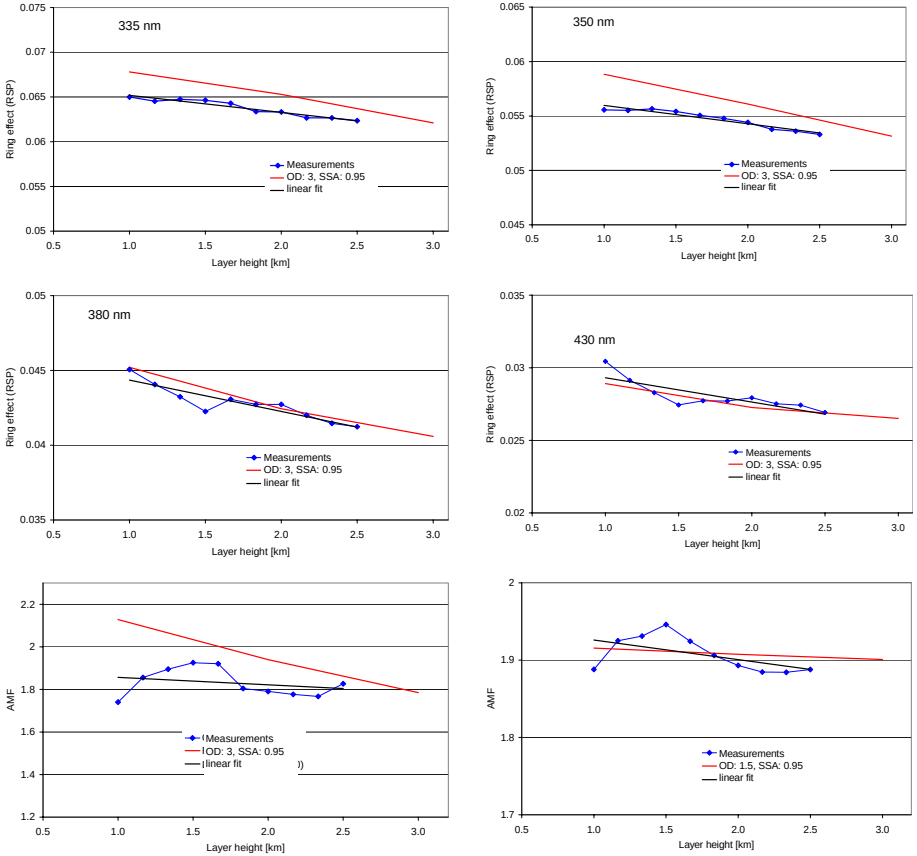

Fig. 20. Observed (blue dots) and simulated dependency of the Ring effect and the O_4 and O_2 absorption on the aerosol layer height over the area south of Beijing on 17 September 2006 (see Fig. 19). For the radiative transfer calculations the following properties were assumed: surface albedo: 15% (630 nm) and 5% (all other wavelengths), aerosol SSA: 0.95; *g*: 0.68, AOD: 1.5 (630 nm) and 3 (all other wavelengths).

AMTD
3, 3535–3599, 2010

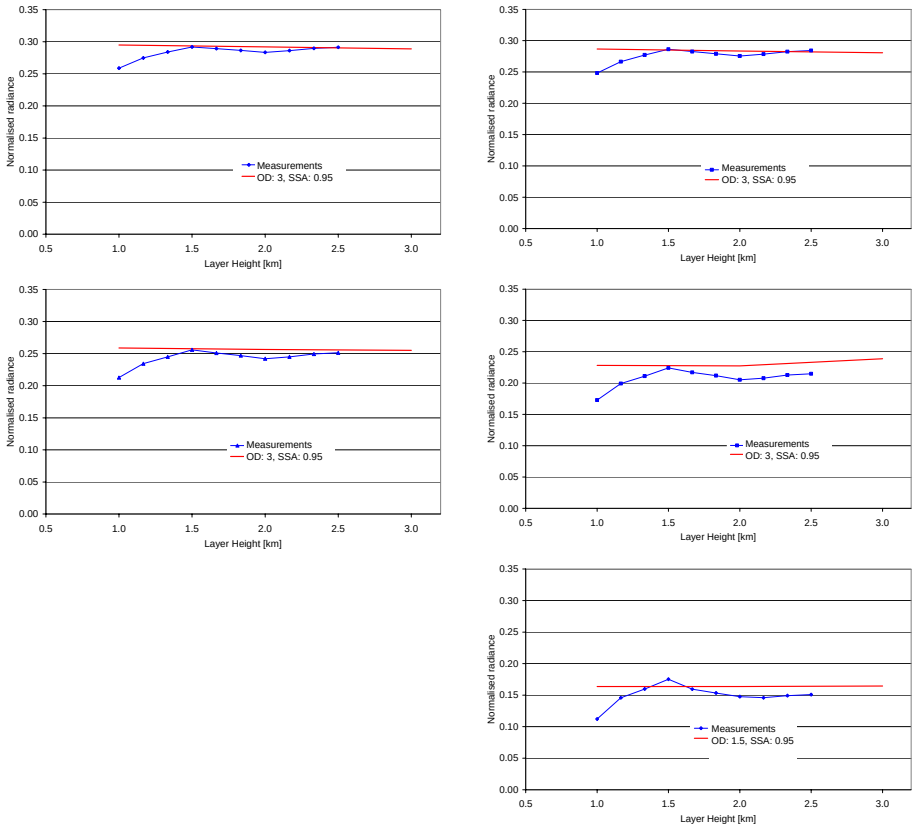

Fig. 21. Observed (blue dots and lines) and simulated (red lines) dependency of the normalised radiance on the aerosol layer height over the area south of Beijing on 17 September 2006 (see Fig. 19). For the radiative transfer calculations the following properties were assumed: surface albedo: 15% (630 nm) and 5% (all other wavelengths), aerosol SSA: 0.95; *g*: 0.68, AOD: 1.5 (630 nm) and 3 (all other wavelengths).

AMTD
3, 3535–3599, 2010

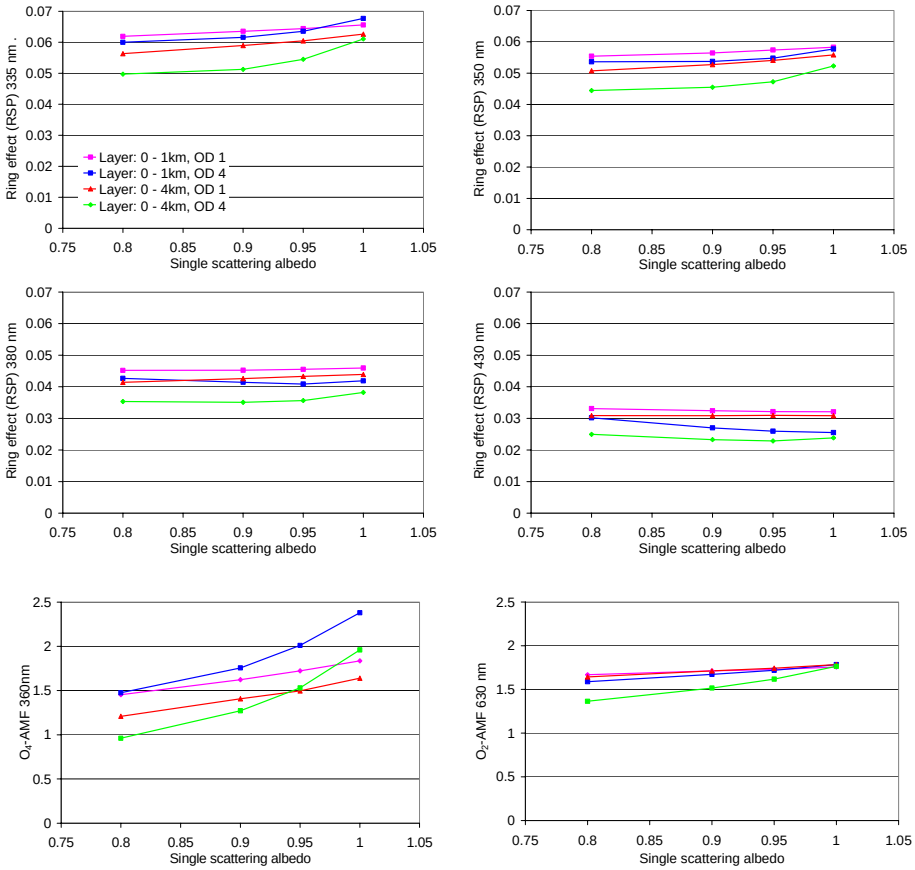

Fig. 22. Dependence of the Ring effect and the O_2 and O_4 absorptions on the aerosol single scattering albedo. The calculations are performed for SZA of 30° and a viewing angle of −90° (nadir geometry). The aerosol asymmetry parameter was assumed to be 0.68.

AMTD
3, 3535–3599, 2010

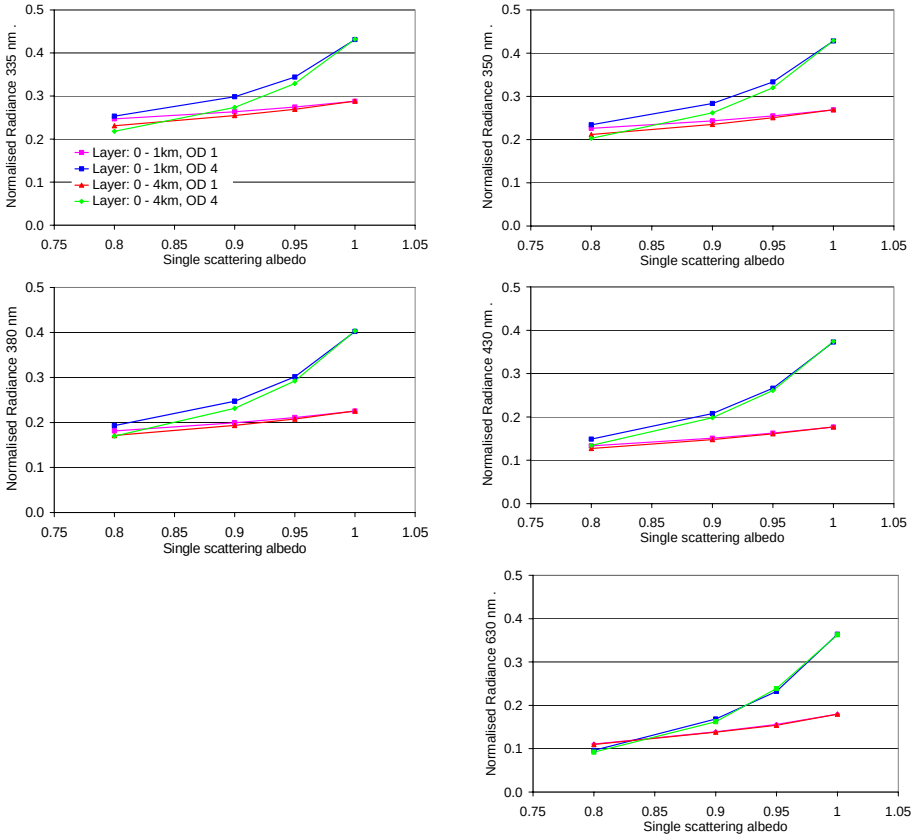

Fig. 23. Dependence of the normalised radiance on the aerosol single scattering albedo. The calculations are performed for SZA of 30° and a viewing angle of −90° (nadir geometry). The aerosol asymmetry parameter was assumed to be 0.68.

AMTD
3, 3535–3599, 2010

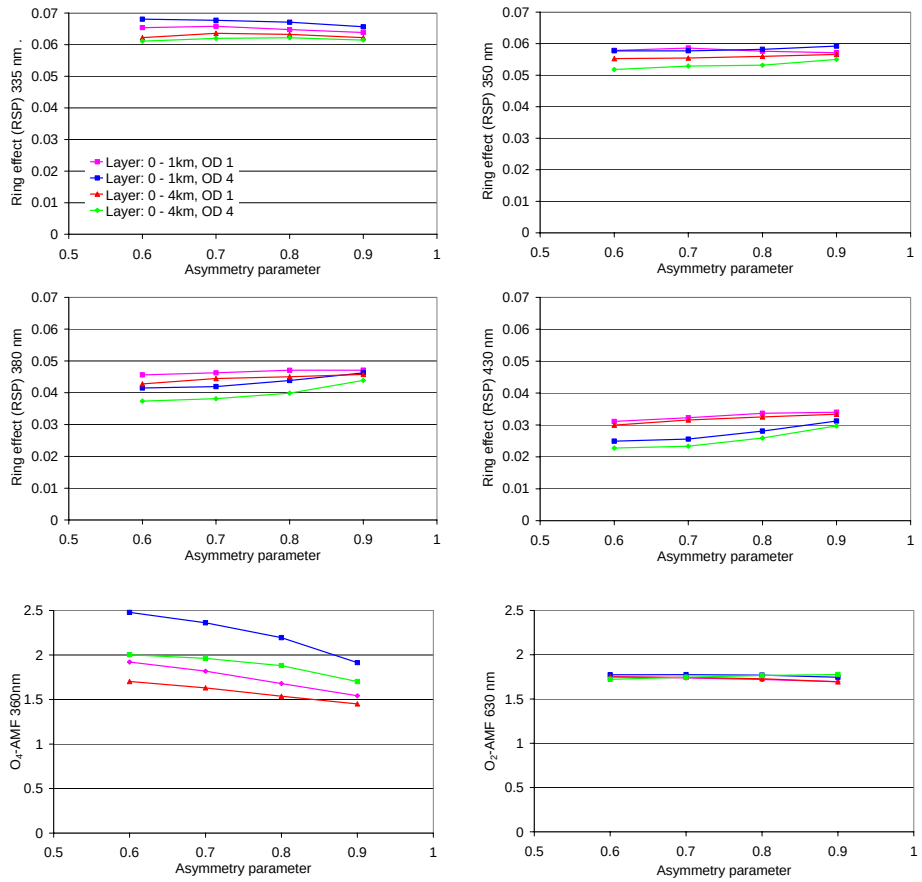

Fig. 24. Dependence of the Ring effect and the O_2 and O_4 absorptions on the aerosol asymmetry parameter g. The calculations are performed for aerosol single scattering albedo of 1, SZA of 30°, and a viewing angle of −90° (nadir geometry).

AMTD
3, 3535–3599, 2010

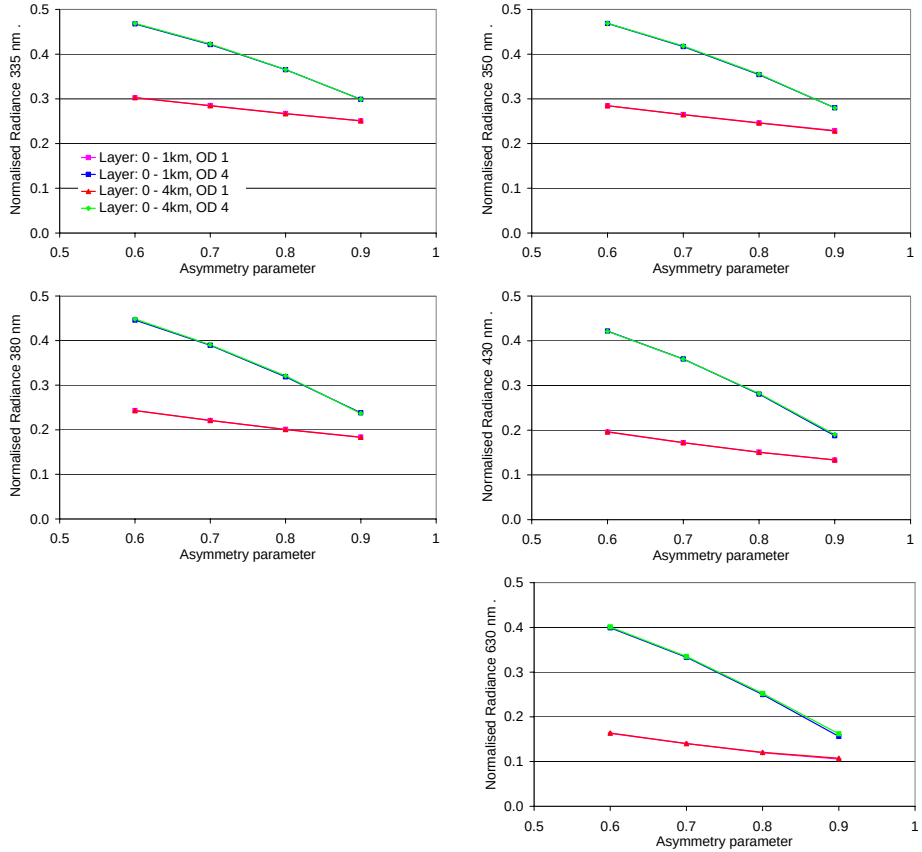

Fig. 25. Dependence of the normalised radiance on the aerosol asymmetry parameter g. The calculations are performed for aerosol single scattering albedo of 1, SZA of 30°, and a viewing angle of −90° (nadir geometry).

AMTD
3, 3535–3599, 2010

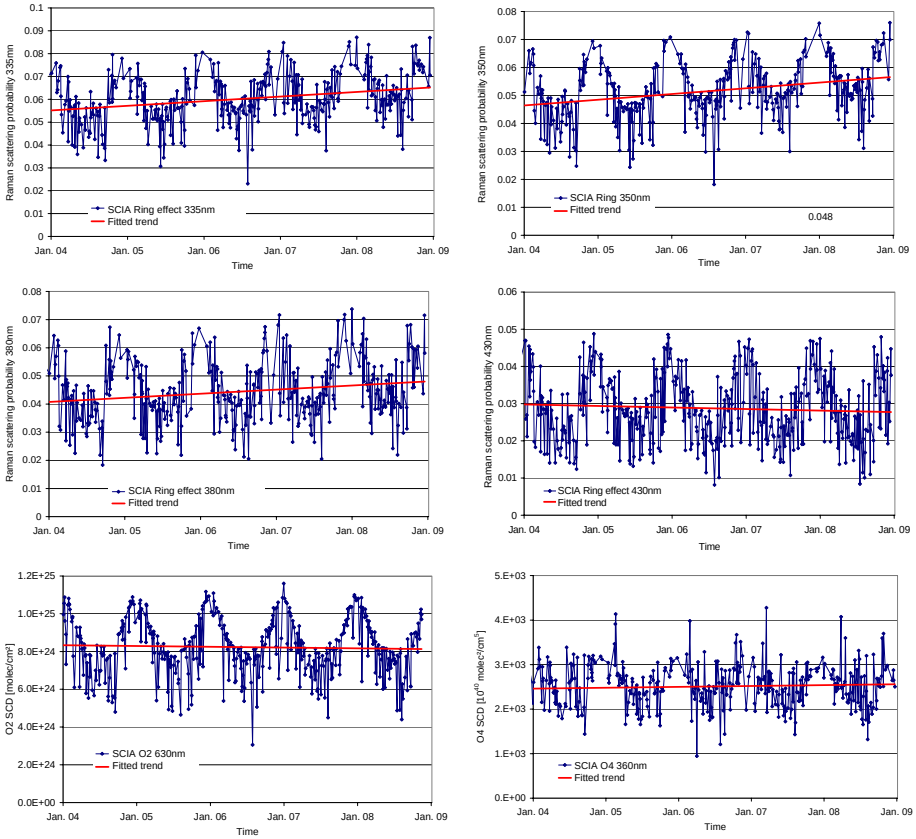

Fig. A1. Time series (2004–2008) of the Ring effect and the O_2 and O_4 absorptions over Beijing. Especially the Ring effect observations in the UV show a strong temporal trend, which is fitted by a regression line (red).

AMTD
3, 3535–3599, 2010

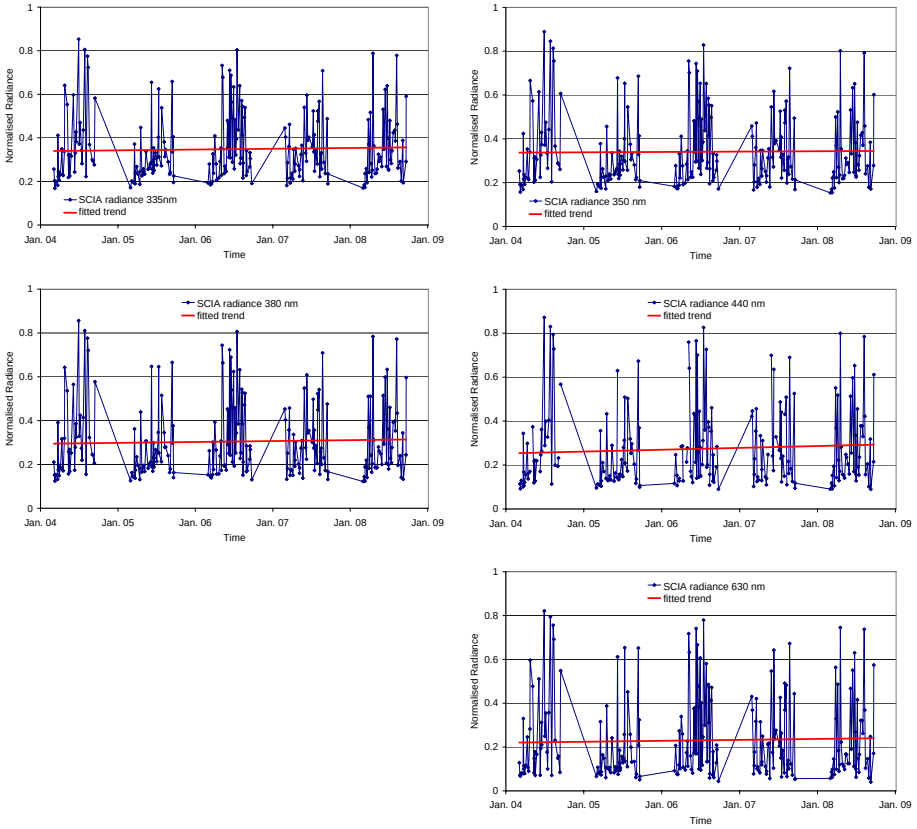

Fig. A2. Time series (2004–2008) of the normalised radiance over Beijing. The temporal trend is fitted by a regression line (red). The data were corrected using M-Factors, hence the trend is not very strong.

AMTD
3, 3535–3599, 2010

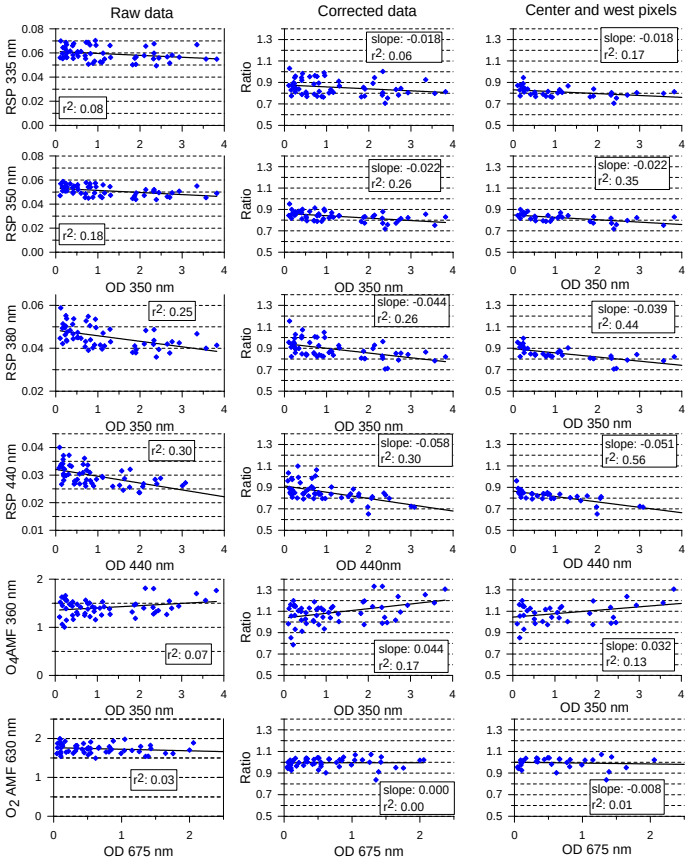

Fig. B1. Correlation analyses of the Ring effect and O_2 and O_4 absorption over Beijing and the AOD (from AERONET observations). The left column presents "raw" data for all cloud-free observations. The middle panel shows the same data after correction of long term trend and SZA dependence. The right panel shows the results after excluding the most eastern pixels.

AMTD
3, 3535–3599, 2010

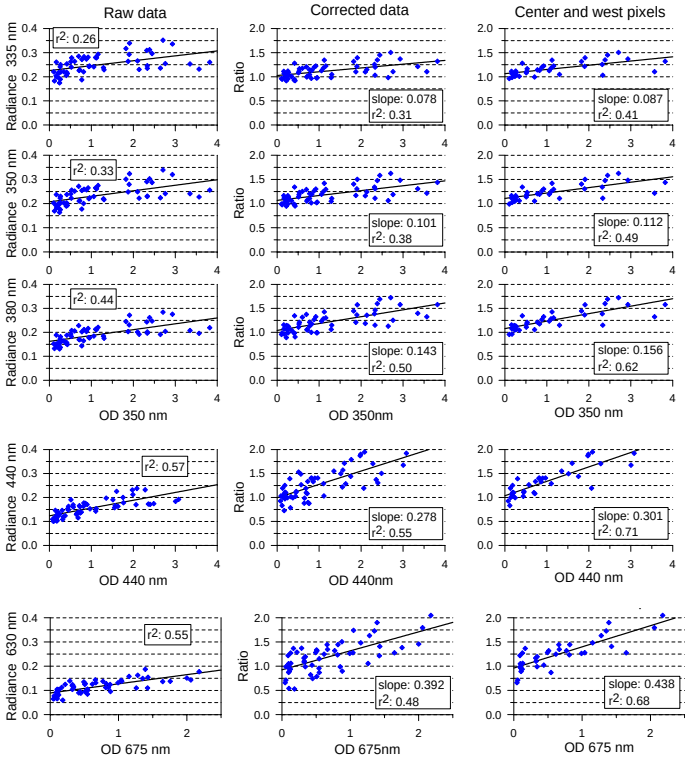

Fig. B2. Correlation analyses of the normalised radiance over Beijing and the AOD (from AERONET observations). The left column presents "raw" data for all cloud-free observations. The middle panel shows the same data after correction of long term trend and SZA dependence. The right panel shows the results after excluding the most eastern pixels.

AMTD
3, 3535–3599, 2010

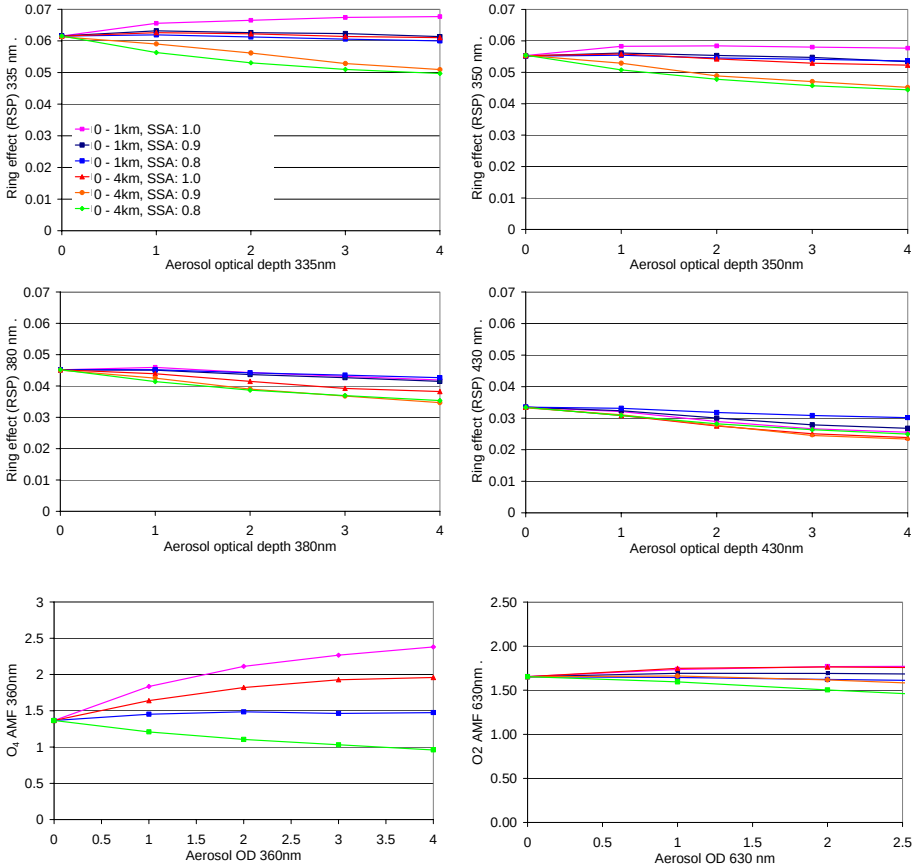

Fig. B3. Dependence of the Ring effect and the O_2 and O_4 absorptions on the AOD. The calculations are performed for SZA of 30° and a viewing angle of −90° (nadir geometry). For 630 nm the surface albedo was set to 10%; for all other wavelengths it was set to 5%. The aerosol asymmetry parameter was assumed to be 0.68.

AMTD
3, 3535–3599, 2010

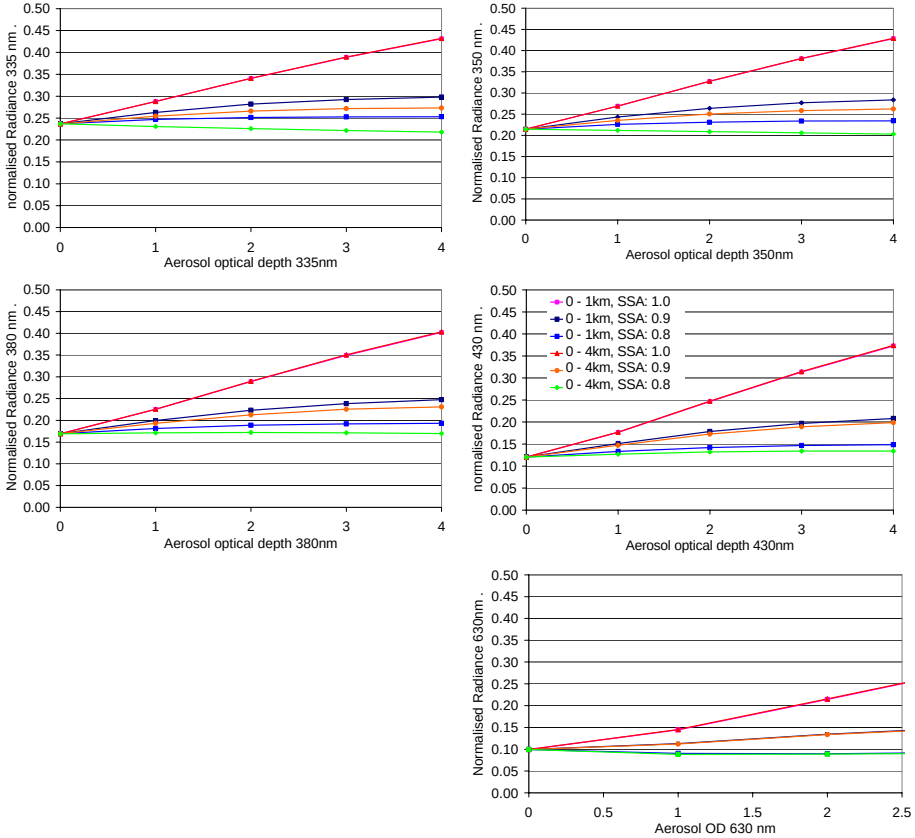

Fig. B4. Dependence of the normalised radiance on the AOD. The calculations are performed for SZA of 30° and a viewing angle of −90° (nadir geometry). For 630 nm the surface albedo was set to 10%; for all other wavelengths it was set to 5%. The aerosol asymmetry parameter was assumed to be 0.68.

AMTD
3, 3535–3599, 2010